The Astrophysical Journal, 769:130 (16pp), 2013 June 1 doi:10.1088/0004-637X/769/2/130

DISCOVERY OF A COSMOLOGICAL, RELATIVISTIC OUTBURST VIA ITS RAPIDLY FADING OPTICAL EMISSION

S. Bradley Cenko[1], S. R. Kulkarni[2], Assaf Horesh[2], Alessandra Corsi[3,4], Derek B. Fox[5], John Carpenter[2], Dale A. Frail[6], Peter E. Nugent[1,7], Daniel A. Perley[2,19], D. Gruber[8], Avishay Gal-Yam[9,20], Paul J. Groot[2,10], G. Hallinan[2], Eran O. Ofek[9], Arne Rau[8], Chelsea L. MacLeod[11], Adam A. Miller[1], Joshua S. Bloom[1], Alexei V. Filippenko[1], Mansi M. Kasliwal[12], Nicholas M. Law[13], Adam N. Morgan[1], David Polishook[14], Dovi Poznanski[15], Robert M. Quimby[16], Branimir Sesar[2], Ken J. Shen[1,7,21], Jeffrey M. Silverman[1,17], and Assaf Sternberg[18,22]

[1] Department of Astronomy, University of California, Berkeley, CA 94720-3411, USA; cenko@astro.berkeley.edu
[2] Cahill Center for Astrophysics, California Institute of Technology, Pasadena, CA 91125, USA
[3] LIGO Laboratory, California Institute of Technology, MS 100-36, Pasadena, CA 91125, USA
[4] Physics Department, George Washington University, 725 21st Street, NW Washington, DC 20052, USA
[5] Department of Astronomy & Astrophysics, Pennsylvania State University, University Park, PA 16802, USA
[6] National Radio Astronomy Observatory, P.O. Box O, Socorro, NM 87801, USA
[7] Lawrence Berkeley National Laboratory, Berkeley, CA 94720, USA
[8] Max Planck Institute for Extraterrestrial Physics, Giessenbachstrasse, Postfach 1312, D-85748 Garching, Germany
[9] Benoziyo Center for Astrophysics, Weizmann Institute of Science, 76100 Rehovot, Israel
[10] Department of Astrophysics/IMAPP, Radboud University Nijmegen, 6500 GL Nijmegen, The Netherlands
[11] Physics Department, United States Naval Academy, 572c Holloway Road, Annapolis, MD 21402, USA
[12] Observatories of the Carnegie Institution for Science, 813 Santa Barbara St., Pasadena, CA 91101, USA
[13] Dunlap Institute of Astronomy & Astrophysics, University of Toronto, 50 St. George Street, Toronto, ON M5S 3H4, Canada
[14] Department of Earth, Atmospheric, and Planetary Sciences, Massachusetts Institute of Technology, Cambridge, MA 02139, USA
[15] School of Physics and Astronomy, Tel-Aviv University, Tel Aviv 69978, Israel
[16] Kavli IPMU, University of Tokyo, 5-1-5 Kashiwanoha, Kashiwa City, Chiba 277-8583, Japan
[17] Department of Astronomy, University of Texas, Austin, TX 78712-0259, USA
[18] Max Planck Institute for Astrophysics, Karl Schwarzschild St. 1, D-85741 Garching, Germany
Received 2013 January 20; accepted 2013 April 15; published 2013 May 14

ABSTRACT

We report the discovery by the Palomar Transient Factory (PTF) of the transient source PTF11agg, which is distinguished by three primary characteristics: (1) bright ($R_{\rm peak} = 18.3$ mag), rapidly fading ($\Delta R = 4$ mag in $\Delta t = 2$ days) optical transient emission; (2) a faint ($R = 26.2 \pm 0.2$ mag), blue ($g' - R = 0.17 \pm 0.29$ mag) quiescent optical counterpart; and (3) an associated year-long, scintillating radio transient. We argue that these observed properties are inconsistent with any known class of Galactic transients (flare stars, X-ray binaries, dwarf novae), and instead suggest a cosmological origin. The detection of incoherent radio emission at such distances implies a large emitting region, from which we infer the presence of relativistic ejecta. The observed properties are all consistent with the population of long-duration gamma-ray bursts (GRBs), marking the first time such an outburst has been discovered in the distant universe independent of a high-energy trigger. We searched for possible high-energy counterparts to PTF11agg, but found no evidence for associated prompt emission. We therefore consider three possible scenarios to account for a GRB-like afterglow without a high-energy counterpart: an "untriggered" GRB (lack of satellite coverage), an "orphan" afterglow (viewing-angle effects), and a "dirty fireball" (suppressed high-energy emission). The observed optical and radio light curves appear inconsistent with even the most basic predictions for off-axis afterglow models. The simplest explanation, then, is that PTF11agg is a normal, on-axis long-duration GRB for which the associated high-energy emission was simply missed. However, we have calculated the likelihood of such a serendipitous discovery by PTF and find that it is quite small (≈2.6%). While not definitive, we nonetheless speculate that PTF11agg may represent a new, more common (>4 times the on-axis GRB rate at 90% confidence) class of relativistic outbursts lacking associated high-energy emission. If so, such sources will be uncovered in large numbers by future wide-field optical and radio transient surveys.

Key words: gamma-ray burst: general – stars: flare – supernovae: general

Online-only material: color figures

1. INTRODUCTION

From accreting stellar-mass black holes in our Galaxy to distant active galactic nuclei (AGNs) and gamma-ray bursts (GRBs), outflow velocities approaching the speed of light are common in nature. Indeed, the number of known sources capable of generating relativistic ejecta has expanded in recent years to include a core-collapse supernova without an accompanying GRB (SN 2009bb; Soderberg et al. 2010), as well as the presumed tidal disruption of a star by a supermassive black hole (Levan et al. 2011; Bloom et al. 2011; Zauderer et al. 2011; Burrows et al. 2011; Cenko et al. 2012). With revolutionary new time-domain facilities slated to come online in the coming decade, even more exotic examples will surely be uncovered.

Time-variable high-energy emission (X-rays and γ-rays) tends to be the hallmark of such relativistic outflows. Yet there is good reason to expect that some relativistic outbursts may lack a detectable high-energy signature. In the case of GRBs,

[19] Hubble Fellow.
[20] Kimmel Investigator.
[21] Einstein Fellow.
[22] Minerva Fellow.

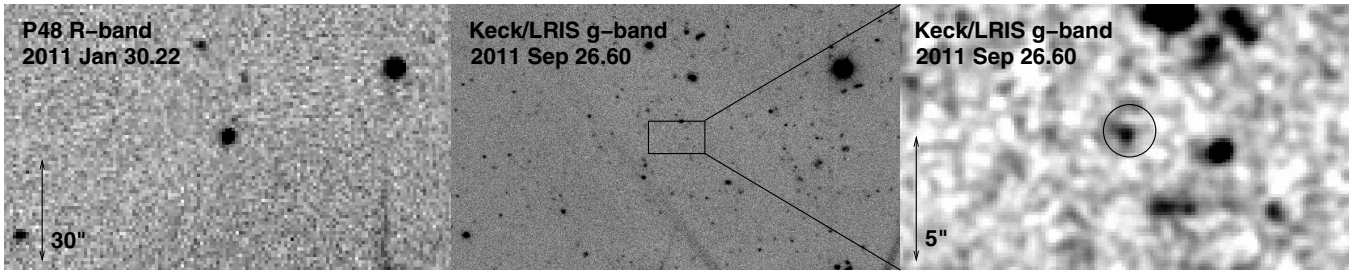

Figure 1. Optical imaging of the field of PTF11agg. The P48 discovery (*R*-band) image is shown in the left panel. Follow-up Keck/LRIS *g*-band observations, obtained on 2011 September 26, are displayed in the center (wider field) and right (zoomed in) panels. The location of PTF11agg, as determined from our P48 imaging, is indicated with a solid circle (1″ radius; note that this is significantly larger than the astrometric uncertainty in our alignment between the Keck/LRIS and P48 images, which is ∼50 mas in each coordinate). A faint, unresolved source consistent with the location of PTF11agg is detected in both our *g*-band and *R*-band (not shown) images. All images are oriented with north facing up and east to the left.

for example, the most mundane possibility is a lack of sky coverage: the most sensitive high-energy GRB detectors cover only a fraction of the sky at any given time. But other, more interesting possibilities exist, including viewing-angle effects (Rhoads 1997; Perna & Loeb 1998; Nakar et al. 2002) and some physical process suppressing the high-energy emission entirely (Dermer et al. 2000; Huang et al. 2002; Rhoads 2003). The search at longer wavelengths for these "orphan" (i.e., off-axis) afterglows or "dirty fireballs" has remained one of the most sought-after goals in the GRB field for more than a decade.

In this work, we report the discovery by the Palomar Transient Factory (PTF) of PTF11agg, a rapidly fading optical transient associated with a year-long, scintillating radio counterpart. The detection of a faint, blue, quiescent optical source at the transient location suggests a cosmological origin for the transient (i.e., well beyond the Milky Way and any nearby galaxies). At such distances, the observed radio emission requires the presence of relativistic ejecta.

Throughout this work, we adopt a standard ΛCDM cosmology with $H_0 = 71\,\mathrm{km\,s^{-1}\,Mpc^{-1}}$, $\Omega_\mathrm{m} = 0.27$, and $\Omega_\Lambda = 1 - \Omega_\mathrm{m} = 0.73$ (Spergel et al. 2007). All quoted uncertainties are 1σ (68%) confidence intervals unless otherwise noted, and UT times are used throughout. Reported optical magnitudes are in the AB system (Oke & Gunn 1983). We have corrected the reported optical and near-infrared (NIR) photometry for a foreground Galactic extinction of $E(B-V) = 0.044$ mag (Schlegel et al. 1998), using the extinction law from Cardelli et al. (1989).

2. DISCOVERY AND BASIC ANALYSIS

2.1. Optical/Near-infrared

2.1.1. Observations

Regular monitoring observations of field 100033 (centered at $\alpha = 08^\mathrm{h}23^\mathrm{m}32\overset{\mathrm{s}}{.}42$, $\delta = +21^\circ33'34\overset{''}{.}5$, with a total on-sky area of 7.2 deg^2) were obtained with the Palomar 48 inch Oschin telescope (P48) equipped with the refurbished CFHT12k camera (Rahmer et al. 2008) as part of a program to study stellar variability in Praesepe (the Beehive Cluster; Agüeros et al. 2011) by the PTF (Law et al. 2009; Rau et al. 2009). Over 500 individual P48 frames, each with an exposure time of 60 s, were obtained over the period from 2009 November through 2012 March. All P48 images were obtained with a Mould *R*-band filter, which is similar to the r' filter from the Sloan Digital Sky Survey (SDSS; Aihara et al. 2011), but offset by ∼27 Å redward (Ofek et al. 2012).

In an image beginning at 5:17:11 on 2011 January 30, we detected a bright but short-lived optical flare at the (J2000.0) location $\alpha = 08^\mathrm{h}22^\mathrm{m}17\overset{\mathrm{s}}{.}195$, $\delta = +21^\circ37'38\overset{''}{.}26$, with a 1σ astrometric uncertainty of 70 mas in each coordinate (Figure 1). This source was subsequently dubbed PTF11agg by our automated discovery and classification pipeline (Bloom et al. 2012). Our P48 photometry of PTF11agg, calculated with respect to nearby point sources from SDSS, is presented in Table 1.

The peak observed magnitude, obtained in our first image of the field on 2011 January 30, was measured to be $R = 18.26 \pm 0.05$ mag. In the next 10 P48 images of the field, all obtained on 2011 January 30, the source is seen to decay by 1.2 mag in the *R* band. A faint detection is also obtained by co-adding all P48 images from 2011 February 1 ($R = 22.15 \pm 0.33$ mag). The resulting P48 *R*-band light curve is plotted in Figure 2. All subsequent P48 images result in non-detections at this location.

Examining our pre-outburst (i.e., before 2011 January 30) P48 imaging, we find no evidence for emission at this location in any individual frames (extending back in time to 2009 November). The typical limiting magnitude for an individual P48 image is $R \gtrsim 20$ mag. Stacking all frames from 2011 January 29 (i.e., the day preceding discovery), we limit the optical emission at the location of PTF11agg to $R > 21.9$ mag. Similarly, co-adding all pre-outburst P48 images results in a non-detection with $R > 23.7$ mag.

Deep optical imaging of the location of PTF11agg was obtained at late times ($\Delta t > 1$ month) with the Low Resolution Imaging Spectrometer (LRIS; Oke et al. 1995) mounted on the 10 m Keck I telescope (g'- and *R*-band filters), and the Inamori-Magellan Areal Camera and Spectrograph (IMACS; Dressler et al. 2011) mounted on the 6.5 m Magellan-Baade telescope at Las Campanas Observatory (*I*-band filter).

In our deepest epoch of post-outburst optical imaging (2011 September 26 with Keck/LRIS, or $\Delta t = 240$ days), we identify a faint, unresolved (in 0.″6 seeing) source in g' and *R* at (J2000.0) coordinates $\alpha = 08^\mathrm{h}22^\mathrm{m}17\overset{\mathrm{s}}{.}202$, $\delta = +21^\circ37'38\overset{''}{.}26$ (Figure 1). Given the uncertainty in the astrometric tie between the Keck/LRIS and P48 imaging (50 mas in each coordinate), the observed 90 mas radial offset is not statistically significant (null probability of 0.17). Co-adding Keck/LRIS images of the field of PTF11agg from several individual nights with less ideal conditions (2011 March 4, March 12, and April 27), we can recover an object at this location with similar brightness in both g' and *R*. No emission is detected at this location in the *I*-band IMACS images to $I > 25.2$ mag.

We obtained NIR imaging of the location of PTF11agg with the 1.3 m Peters Automated InfraRed Imaging TELescope

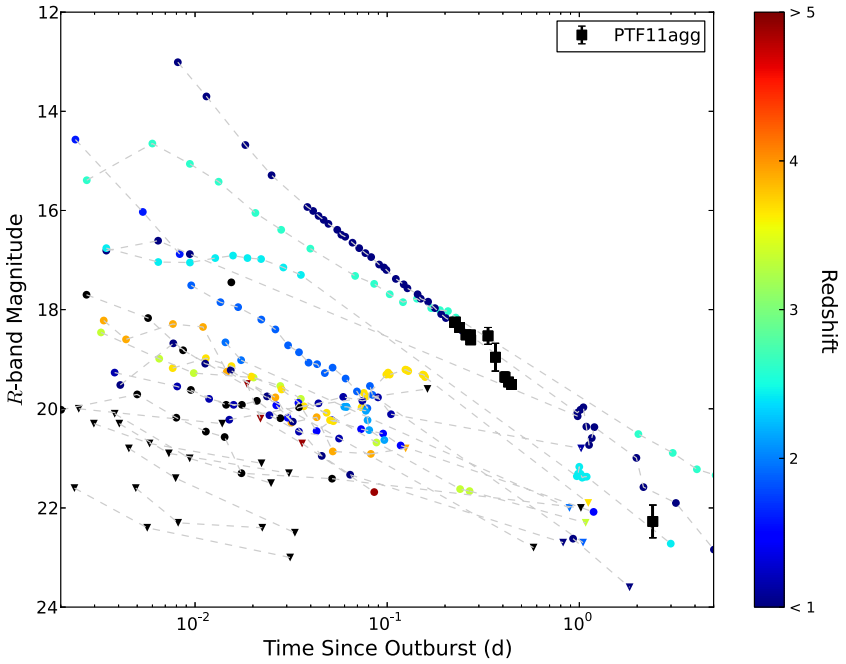

Figure 2. Optical light curve of PTF11agg, compared with a representative sample of afterglows of long-duration GRBs discovered by the *Swift* satellite (Cenko et al. 2009). The *Swift* GRBs are color-coded by redshift; small black points indicate GRBs with unknown distance. The observed power-law decline from PTF11agg ($\alpha = 1.66$) is consistent with GRB afterglow observations at $\Delta t \approx 1$ day after the burst. Though at the high end of the observed brightness distribution at $\Delta t \approx 0.2$ days, a sizeable fraction ($\sim$10%) of *Swift* events have a comparable *R*-band magnitude at $\Delta t \approx 1$ day. The inverted triangles mark 3σ upper limits.

(A color version of this figure is available in the online journal.)

Table 1
Optical/Near-infrared Observations of PTF11agg

Date (MJD)	Telescope/Instrument	Filter	Exposure Time (s)	Magnitude
55590.30519	P48/CFHT12k	*R*	540	>21.9
55591.22026	P48/CFHT12k	*R*	60	18.26 ± 0.05
55591.22245	P48/CFHT12k	*R*	60	18.25 ± 0.04
55591.23391	P48/CFHT12k	*R*	60	18.36 ± 0.05
55591.25326	P48/CFHT12k	*R*	60	18.51 ± 0.08
55591.26691	P48/CFHT12k	*R*	60	18.51 ± 0.04
55591.26800	P48/CFHT12k	*R*	60	18.61 ± 0.06
55591.33081	P48/CFHT12k	*R*	60	18.53 ± 0.17
55591.36188	P48/CFHT12k	*R*	60	18.96 ± 0.28
55591.40604	P48/CFHT12k	*R*	60	19.36 ± 0.10
55591.42439	P48/CFHT12k	*R*	60	19.46 ± 0.09
55591.43978	P48/CFHT12k	*R*	60	19.51 ± 0.10
55593.40775	P48/CFHT12k	*R*	420	22.15 ± 0.33
55594.23819	P48/CFHT12k	*R*	300	>21.2
55621.19100	PAIRITEL	*H*	2246	>20.4
55621.19100	PAIRITEL	*J*	2246	>20.6
55621.19100	PAIRITEL	K_s	2246	>19.7
55624.49–55678.28	Keck I/LRIS	g'	6680	26.63 ± 0.33
55624.49–55678.28	Keck I/LRIS	*R*	5700	26.28 ± 0.28
55830.60259	Keck I/LRIS	g'	2100	26.34 ± 0.19
55830.59849	Keck I/LRIS	*R*	2160	26.17 ± 0.22
55944.22461	Magellan/IMACS	*I*	2400	>25.2
56014.27324	P200/WIRC	K_s	1200	>22.6

(PAIRITEL; Bloom et al. 2006) on 2011 March 1 ($\Delta t = 30$ days). A total exposure time of 2246 s was obtained simultaneously in the *J*, *H*, and K_s filters. Raw data files were processed using standard NIR reduction methods via PAIRITEL Pipeline III (C. Klein et al., in preparation), and resampled using SWarp (Bertin et al. 2002) to create $1\farcs0$ pixel^{-1} images for final photometry.

We also observed the location of PTF11agg with the Wide-Field Infrared Camera (WIRC; Wilson et al. 2003) mounted on the 5 m Hale telescope at Palomar Observatory. The images were obtained in the K_s filter on 2012 March 28 ($\Delta t = 423$ days) for a total exposure time of 1200 s. The individual frames were reduced using a custom pipeline within the IRAF environment (Tody 1986). Both the PAIRITEL and WIRC images were

calibrated with respect to bright field stars from the Two Micron All Sky Survey (2MASS; Skrutskie et al. 2006).

No emission was detected at the location of PTF11agg in any of the NIR bandpasses. The most constraining limits come from the WIRC observations ($K_s > 22.6$ mag).

A full listing of our optical and NIR photometry is presented in Table 1. To convert the Vega-based measurements from 2MASS to the AB system, we have used the offsets derived by Blanton & Roweis (2007).

2.1.2. Constraints on the Decay Index and Optical Outburst Onset

We fit the observed P48 detections on 2011 January 30 and February 1 to a power-law model of the form $f_\nu = f_0(t - t_0)^{-\alpha}$, where f_ν is the flux density (in μJy), t_0 is the time of the outburst onset, α is the power-law index, and f_0 is the flux density at a fiducial time (t_0 + 1 s). We find best-fit values of $\alpha = 1.66 \pm 0.35$ and $t_0 = 23{:}34$ UT (± 1.7 hr) on 2011 January 29. We note that the inferred outburst onset t_0 occurs 16.6 hr after the preceding P48 non-detection on 2011 January 29 (Table 1).

In the event that PTF11agg is a *bona fide* GRB-like afterglow (Section 4), an alternative constraint on the explosion date can be derived by comparing the peak brightness of PTF11agg with the observed distribution of GRB optical afterglows. Using the comprehensive sample from Kann et al. (2010), an observed magnitude of $R = 18.26$ at discovery implies an age of $\Delta t \lesssim 0.5$ days (Figure 2). Put differently, the brightest known GRB optical afterglows reach an observed magnitude of $R \approx 18$ approximately 12 hr after the onset of the high-energy emission. Together with the P48 non-detection on 2011 January 29.31, we can conservatively constrain the outburst onset to fall within the window from ~17:00 on 2011 January 29 to 5:17 on 2011 January 30 (55590.71–55591.22 MJD).

While the overall power-law fit quality is acceptable ($\chi^2 = 8.1$ for 9 degrees of freedom), we caution that the early optical light curves of GRBs rarely exhibit single power-law decays (Panaitescu & Vestrand 2008; Rykoff et al. 2009; Oates et al. 2009). In the event that the outburst occurred later than our derived t_0, the true power-law index will be smaller than what we have inferred, and more consistent with most previously observed GRB optical afterglows. If the outburst actually occurred earlier, the decay index would steepen somewhat. But temporal indices $\alpha \gtrsim 2.5$ are ruled out based on the non-detection on 2011 January 29.

2.1.3. Likelihood of Quiescent Source Association

Here we wish to estimate $P_{\rm chance}$, the a posteriori likelihood that the coincident quiescent counterpart detected at late times in our Keck/LRIS imaging is unrelated to PTF11agg (i.e., the transient source). We have measured the areal surface density of objects of this brightness in our imaging of field 100033, finding $\sigma(R \leqslant 26.2) = 0.03$ galaxies arcsec^{-2}; we note that this is consistent with the results from Hogg et al. (1997) using entirely different fields. Using 150 mas, or three times the uncertainty in the astrometric tie between the P48 and Keck/LRIS images, as our search radius, and following Bloom et al. (2002), we find that $P_{\rm chance} = 2 \times 10^{-3}$. We therefore consider it highly likely that this source is the quiescent counterpart of PTF11agg; however, we consider alternative possibilities below as well.

2.2. Radio

2.2.1. Observations

We began radio observations of the field of PTF11agg with the National Radio Astronomy Observatory's (NRAO[23]) Karl G. Jansky Very Large Array (VLA; Perley et al. 2011) on 2011 March 11 ($\Delta t = 40$ days). The array was in the "B" configuration until 2011 May 6, then the "BnA" configuration until 2011 June 1, and the "A" configuration thereafter. Over the course of our monitoring, the angular resolution ranged from 0.″3 to 1.″2. The VLA data were reduced with the Astronomical Image Processing System (AIPS).[24] For flux calibration, we used the source 3C 147, while phase calibration was performed using the objects J0823+2223 and J0832+1832. As a check of our flux calibration, we have verified that the flux measurements of our phase calibration sources remain stable throughout the course of our observations.

We observed PTF11agg at high frequencies (mm wavelengths) with the Combined Array for Research in Millimeter-wave Astronomy (CARMA) beginning on 2011 March 14 ($\Delta t = 43$ days) and continuing for approximately one month. For our CARMA observations, the array was in the "D" configuration, and the beam had an angular diameter of 10″. The total bandwidth (lower sideband and upper sideband) was 8 GHz, and the local oscillator frequency was 93.6 GHz. The optical depth at high (230 GHz) frequency ranged from fair ($\tau \approx 0.4$; phase noise ≈50°) on March 14 and April 11, to good ($\tau \approx 0.1$; phase noise ≈40°) on April 7. Data were reduced using standard techniques within the MIRIAD environment (Sault et al. 1995).

A transient radio counterpart was detected with both facilities. The radio counterpart was unresolved (smallest beam size of 190 mas) and consistent with zero circular polarization ($q \lesssim 10\%$) at all epochs. The results of our EVLA and CARMA monitoring are displayed in Table 2, while the 8 GHz light curve is plotted in Figure 3.

2.2.2. Spectral Energy Distribution

To calculate the radio spectral energy distribution (SED), we must interpolate the various observing frequencies to a common epoch. To provide the longest lever arm, we perform this analysis at the two epochs of our 93 GHz CARMA detections: 2011 March 14.05 ($\Delta t \approx 43$ days) and 2011 April 7.03 ($\Delta t \approx 67$ days). We have linearly interpolated flux-density measurements made immediately before and after these epochs at frequencies of 5 and 8 GHz. Due to the relatively sparse coverage at 22 GHz, we have simply adopted the flux density at the closest epoch in time (note that for 2011 March 18 we averaged the two 22 GHz measurements obtained on this day). The resulting SEDs are plotted in Figure 4.

We fit a power law of the form $f_\nu = f_0 \nu^\beta$ to the data, where f_ν is the flux density (in μJy), ν is the observing frequency (in GHz), β is the power-law spectral index, and f_0 is the flux density at a fiducial frequency of 1 GHz. For the first epoch ($\Delta t \approx 43$ days), we find $\beta = 0.28 \pm 0.08$. On the second epoch ($\Delta t \approx 67$ days), we measure $\beta = 0.46 \pm 0.07$. Given the relatively large degree of variability (see below), together with the sparse coverage at high frequencies, we adopt $\beta = 1/3$ as an approximate spectral slope in the radio for the remainder of this work.

[23] The National Radio Astronomy Observatory is a facility of the National Science Foundation (NSF) operated under cooperative agreement by Associated Universities, Inc.

[24] See http://www.aips.nrao.edu/index.shtml.

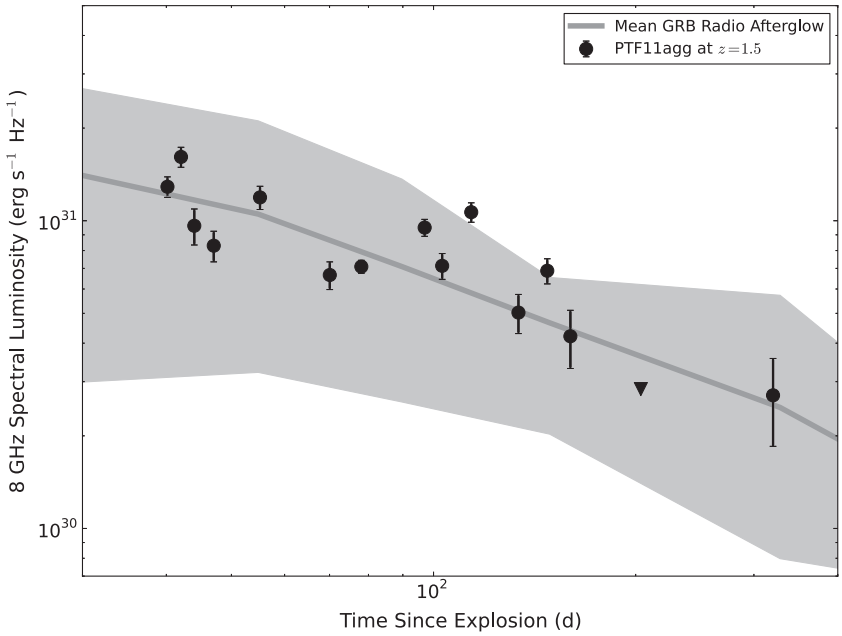

Figure 3. The 8 GHz radio light curve of PTF11agg, at an assumed redshift of 1.5 (in the middle of our allowed range: $0.5 \lesssim z \lesssim 3.0$; Section 4.1). For comparison, we have plotted the mean long-duration GRB radio light curve (solid gray line), as well as the 25%–75% distribution (gray shaded region; Chandra & Frail 2012). The variability superposed on the secular decline is likely due to interstellar scattering by electrons in the Milky Way, and is not intrinsic to the source. For comparison, at $z = 0.5$, the 8 GHz spectral luminosity would be a factor of 15 smaller, while at $z = 3.0$ a factor of 6 larger, than the values plotted here. The inverted triangle marks a 3σ upper limit.

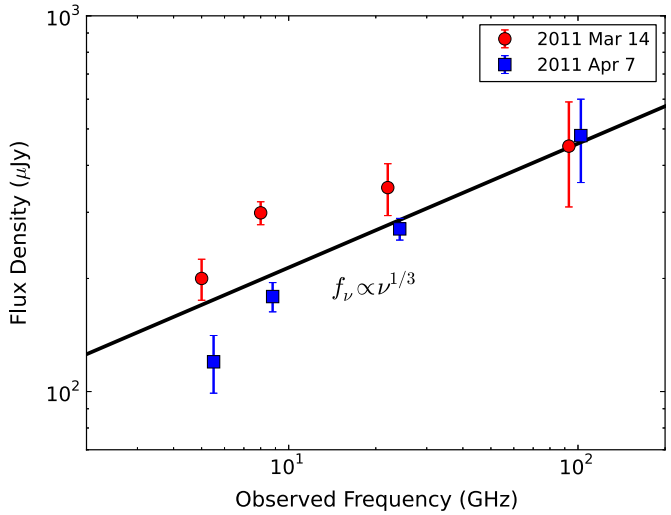

Figure 4. PTF11agg SED at radio frequencies. The observations at lower frequencies have been interpolated to common epochs ($\Delta t \approx 43$ and 67 days) to match the times of our CARMA observations.

(A color version of this figure is available in the online journal.)

2.2.3. Angular Source Size

The presence of nonthermal radio emission provides two powerful and independent means to constrain the angular size of the emitting region. To begin, the brightness temperature (T_B) of an incoherent radio emitter cannot exceed its equipartition value of $T_{B,\rm eq} \approx 10^{11}$ K (Readhead 1994; Kulkarni et al. 1998). The brightness temperature is given by

$$T_B = \frac{c^2}{2k_B\nu^2}\frac{f_\nu}{\pi\Theta^2}, \quad (1)$$

where c is the speed of light, k_B is Boltzmann's constant, ν is the observing frequency, f_ν is the observed flux density, and Θ is the angular diameter of the emitting region. Adopting $T_B \lesssim 10^{11}$ K in Equation (1) thus implies a lower limit on the angular diameter of the source:

$$\Theta \gtrsim 2.1 \left(\frac{f_\nu}{\mu\rm Jy}\right)^{1/2} \left(\frac{\nu}{\rm GHz}\right)^{-1} \mu\rm as. \quad (2)$$

As can be seen from Equation (2), the strictest lower limits on the size of the emitting region are derived from observations at the lowest frequencies (assuming a power-law spectral index $\beta < 2$). Using our 4.5 GHz observation on 2011 March 13, we find $\Theta > 7\,\mu$as. Most of our early observations at 5 and 8 GHz yield comparable (though slightly less strict) limits.

Separately, we can constrain the angular size of the source from the detection of interstellar scattering and scintillation (ISS; Rickett 1990). To quantify the degree of variation induced by the scattering electrons, we calculate the modulation index,

$$m_p(\nu) = \frac{\sqrt{V(f_\nu) - \langle\sigma^2\rangle}}{\langle f_\nu\rangle}, \quad (3)$$

where $V(f_\nu)$ is the variance of the flux density (with respect to an assumed model), $\langle\sigma^2\rangle$ is the average of the square of the individual measurement uncertainties, and $\langle f_\nu\rangle$ is the average of the flux density.

We calculated the modulation indices at 5 and 8 GHz, neglecting higher frequencies due to the relative lack of observations. We fit the light curves at both frequencies to a power-law model of the form $f_\nu = f_0(t - t_0)^{-\alpha}$, finding best-fit temporal indices of $\alpha_{5\,\rm GHz} = -0.09 \pm 0.13$ (i.e., consistent with no temporal evolution) and $\alpha_{8\,\rm GHz} = 0.56 \pm 0.06$. This power-law model then forms the reference which we use to calculate the variance at each frequency. In this manner, we find $m_p(5\ \rm GHz) = 0.42$ and $m_p(8\ \rm GHz) = 0.26$.

We use the Galactic electron density distribution model of Cordes & Lazio (2002) to derive the relevant ISS parameters,

Table 2
Radio Observations of PTF11agg

Date (2011 UT)	Observatory	Frequency (GHz)	Integration Time (minutes)	Flux Density (μJy)
Mar 11.27	VLA	8.46	15.5	300 ± 23
Mar 13.12	VLA	4.50	15.5	217 ± 34
Mar 13.12	VLA	7.92	15.5	375 ± 28
Mar 14.05	CARMA	93.5	492.0	450 ± 140
Mar 15.08	VLA	4.50	15.5	183 ± 36
Mar 15.08	VLA	7.92	15.5	224 ± 30
Mar 18.08	VLA	4.50	15.5	58 ± 37
Mar 18.08	VLA	7.92	15.5	171 ± 31
Mar 18.10	VLA	22.46	10.8	237 ± 79
Mar 18.15	VLA	4.50	15.5	93 ± 35
Mar 18.15	VLA	7.92	15.5	215 ± 29
Mar 18.17	VLA	22.46	10.8	460 ± 77
Mar 26.22	VLA	8.46	15.5	277 ± 24
Apr 5.17	VLA	21.8	30.1	271 ± 18
Apr 7.03	CARMA	93.5	378.0	480 ± 120
Apr 10.11	VLA	4.8	13.7	127 ± 21
Apr 10.11	VLA	7.4	13.7	155 ± 16
Apr 11.01	CARMA	93.5	342.0	-40 ± 150
Apr 18.15	VLA	4.8	37.2	81 ± 11
Apr 18.15	VLA	7.4	37.2	165 ± 8
May 6.08	VLA	4.8	13.7	232 ± 18
May 6.08	VLA	7.4	13.7	221 ± 14
May 13.15	VLA	4.8	12.9	117 ± 18
May 13.15	VLA	7.4	12.9	166 ± 16
May 14.03	VLA	21.8	28.5	133 ± 23
May 23.96	VLA	4.8	8.7	191 ± 25
May 23.96	VLA	7.4	8.7	248 ± 18
Jun 1.06	VLA	22.5	26.5	118 ± 20
Jun 12.88	VLA	4.8	13.8	140 ± 26
Jun 12.88	VLA	7.8	13.8	117 ± 17
Jun 26.86	VLA	4.8	14.0	158 ± 19
Jun 26.86	VLA	7.4	14.0	160 ± 15
Jul 9.94	VLA	4.8	14.0	62 ± 23
Jul 9.94	VLA	7.4	14.0	98 ± 21
Aug 21.71	VLA	8.5	37.2	<44
Dec 16.45	VLA	8.4	25.0	63 ± 20

namely ν_0, the transition frequency between the strong and weak scattering regimes. For the line of sight to PTF11agg (Galactic coordinates $l = 202.^{\circ}08$, $b = 29.^{\circ}2$), we find $\nu_0 = 11$ GHz. For a point source, the maximum degree of modulation ($m_p = 1$) will occur at this transition frequency. It is therefore not unreasonable to expect our observations at 5, 8, and (possibly) 22 GHz to suffer from some degree of ISS.

For $\nu_0 = 11$ GHz, our observations at 5 and 8 GHz will be in the strong scattering regime ($\nu < \nu_0$). Furthermore, given the relatively broad bandwidth of our observations ($\Delta\nu/\nu \approx 0.1$), we consider only refractive scintillation. For a point source, the modulation index in the strong, refractive regime is given by (Walker 1998)

$$m_p(\nu) = \left(\frac{\nu}{\nu_0}\right)^{17/30}. \quad (4)$$

For the line of sight to PTF11agg, we therefore expect a significant degree of modulation for a point source at our observing frequencies: $m_p(5\,\mathrm{GHz}) = 0.63$, $m_p(8\,\mathrm{GHz}) = 0.82$.

For an extended source, the observed modulation will be reduced by a factor of $(\Theta_r/\Theta)^{7/6}$, where Θ_r is the size of the Fresnel scattering disk (Walker 1998),

$$\Theta_r = \frac{8}{\sqrt{D\nu_0}}\left(\frac{\nu_0}{\nu}\right)^{11/5}\ \mu\mathrm{as}, \quad (5)$$

where D is the effective distance to the scattering screen ($D = 0.78$ kpc for the line of sight to PTF11agg). If we solve for the angular diameter corresponding to the observed degree of modulation at each frequency, we find $\Theta(8\ \mathrm{GHz}) = 10\ \mu$as and $\Theta(5\ \mathrm{GHz}) = 34\ \mu$as. We therefore conclude that the angular size of the emitting region at $\Delta t \approx 100$ days is $\Theta \approx 20\ \mu$as.

2.3. High Energy

2.3.1. γ-Ray Limits

At the time of discovery, three primary high-energy facilities were monitoring the sky to search for the prompt emission from GRBs. The Third InterPlanetary Network (IPN; Hurley et al. 2010) is a group of nine satellites sensitive to high-energy emission. When multiple satellites detect a GRB, the sky localization can be reconstructed from light travel time constraints. The IPN provides essentially continuous all-sky coverage (i.e., 100% duty cycle), with a sensitivity to fluences (10 keV–5 MeV) of $S_\gamma \gtrsim 6 \times 10^{-7}$ erg cm^{-2} (at 50% efficiency; i.e., half of the GRBs with this fluence are too faint to trigger the IPN detectors). In addition to the IPN, the Gamma-Ray Burst Monitor (GBM; Meegan et al. 2009) on the *Fermi* satellite, and the Burst Alert Telescope (BAT; Barthelmy et al. 2005) on the *Swift* satellite (Gehrels et al. 2004), also regularly discover a large number of GRBs. The GBM detects bursts down to a 8 keV–1 MeV fluence of $S_\gamma \gtrsim 4 \times 10^{-8}$ erg cm^{-2}, but has a field of view of 8.8 sr (the area of the sky unocculted by the Earth in the *Fermi* orbit) and a duty cycle of $\gtrsim$80%. Likewise, the *Swift* BAT has detected events with 15–150 keV fluences as low as 6×10^{-9} erg cm^{-2}, but only observes a field of view of 2 sr with a duty cycle of $\sim$90%. We caution that, for all three facilities, the high-energy fluence required to trigger the on board GRB algorithms depends on the duration of the event; therefore, the above sensitivity limits should be treated only as approximate.

We have searched all three facilities for GRB triggers from the direction of PTF11agg over the time period from 17:00 2011 January 29 to 5:17 2011 January 30 (i.e., the outburst onset window derived in Section 2.1.2). No triggers were reported by any facility in the direction of PTF11agg during this $\sim$12 hr window. We further conducted a search for untriggered events in the GBM data in the energy range 10–300 keV on several different time scales (0.256 s, 0.512 s, 1.024 s, 2.048 s, 4.096 s, and 8.192 s).[25] No potential high-energy counterparts to PTF11agg were found.

Given the field of view and duty cycle of the GBM and BAT, there is a significant likelihood that events below the IPN sensitivity threshold would be missed by both instruments. For example, for a GRB with fluence above the GBM sensitivity level (but below the IPN threshold), the probability of a non-detection from *both* instruments is as high as $\sim$40% (assuming a uniform and independent distribution of sky pointings for the two instruments). Given the relatively large window of time required to search (i.e., multiple *Swift* and *Fermi* orbits), we consider a fluence of $S_\gamma \lesssim 10^{-6}$ erg cm^{-2} (i.e., twice the all-sky IPN sensitivity) a reasonable limit on any high-energy prompt emission associated with PTF11agg. Given the extremely weak correlation between prompt γ-ray fluence and optical afterglow brightness (Nysewander et al. 2009), this limit is consistent with the known properties of GRBs and their afterglows.

[25] Two individual GBM detectors with a significance of 4.0σ and 3.8σ above background were required for a trigger to register in this search.

2.3.2. X-Ray Limits

To search for an X-ray counterpart, we obtained observations of the location of PTF11agg with the X-ray Telescope (XRT; Burrows et al. 2005) on board the *Swift* satellite on 2011 March 13 ($\Delta t = 42$ days). Data were reduced using the automated pipeline described by Butler & Kocevski (2007). No X-ray source is detected at the location of PTF11agg at this time. Assuming a power-law spectrum with a photon index of $\Gamma = 2$, we derive a 3σ upper limit on the 0.3–10 keV flux of $f_X < 8 \times 10^{-14}$ erg cm^{-2} s^{-1}.

Finally, we note that no historical X-ray emission has been reported at this location, either in the *ROSAT* All-Sky Survey (0.1–2.4 keV; Voges et al. 1999) or in any compilations of known Galactic X-ray sources (accessed via the HEASARC[26] and SIMBAD[27] databases).

3. COMPARISON WITH KNOWN GALACTIC TRANSIENTS

The combination of (1) a rapidly fading optical transient ($\Delta R \gtrsim 4$ mag in $\Delta t = 2$ days) and (2) a faint, blue ($g' - R = 0.17 \pm 0.29$ mag), quiescent optical counterpart makes PTF11agg unique amongst the thousands of discoveries by PTF to date. Together with (3) the long-lived ($\Delta t \approx 300$ days) radio emission, here we attempt to simultaneously account for these three distinguishing characteristics.

In order to understand the nature of the emission from PTF11agg, we must constrain its distance. In this section, we first consider a Galactic origin by comparing PTF11agg with known classes of Galactic transients.

Assuming that the faint optical source is associated with PTF11agg (i.e., the quiescent counterpart), the measured color, $g' - R = 0.17 \pm 0.29$ mag, implies a spectral type of $\sim$ F2 ($T_{\rm eff} \approx 7000$ K) for a main-sequence star. More conservatively, adopting our 3σ limit on the color ($g' - R < 1.04$ mag), we can rule out single main-sequence stars with $T_{\rm eff} \lesssim 4500$ K (i.e., cooler than spectral type K4). Given the observed brightness, a main-sequence star hotter than K4 would lie at a distance $d \gtrsim 90$ kpc. This firmly rules out an association with the Praesepe cluster ($d \approx 175$ pc); in fact, only four globular clusters are known to exist at such large distances in the extreme outer halo of the Milky Way (e.g., AM 1 at $d \approx 120$ kpc; Madore & Arp 1979). In addition to the extremely small source densities this far in the halo, the inferred lower limit on the radio luminosity at such a distance ($\nu L_\nu \gtrsim 10^{31}$ erg s^{-1}) is three orders of magnitude larger than the most luminous known stellar radio sources (e.g., RS CVn binaries, FK Com class stars, and Algol-class stars; Güdel 2002).

While a posteriori unlikely, it is nonetheless important to consider that the quiescent optical source may be unrelated to PTF11agg. Absent color information, an optical non-detection, even at the depth of our late-time imaging, is not sufficient to rule out a Galactic origin. With their smaller effective temperatures, low-mass stars and brown dwarfs (in particular ultracool stars, with spectral type later than M7) emit little flux in the optical bandpass. Furthermore, ultracool stars are known to exhibit high-amplitude, short timescale (minutes to hours) optical and radio outbursts that have in the past been mistaken for extragalactic transients (Becker et al. 2004; Kulkarni & Rau 2006; Mahabal et al. 2012; Berger et al. 2012a).

We can use our NIR limits on the quiescent emission at the location of PTF11agg to calculate the minimum distance to an ultracool star as a function of spectral type; in other words, for each spectral type, any object closer than this "detectability" distance would be identified in our NIR imaging. For spectral types later than $\sim$M4, the strongest constraint is provided by our deepest epoch of K_s-band imaging: $K_s > 22.6$ mag. Using the observed K_s-band magnitudes and distance (parallax) measurements for ultracool stars from Dahn et al. (2002) and Patten et al. (2006), we fit a low-order polynomial to calculate the absolute K_s-band magnitude as a function of spectral type, $M_{K_s}(ST)$, where $ST = 5$ for M5, $ST = 12$ for L2, etc. We find the scatter about our derived absolute K_s-band magnitude fit is $\sim$0.30 mag (i.e., 30%) over the range M5–T8. We then convert the observed peak radio flux density ($f_{\nu,\rm peak} \approx 300\,\mu$Jy) to a lower limit on the radio luminosity (νL_ν) using these distance constraints.

The resulting luminosity limits, as a function of spectral type, are plotted in Figure 5. For comparison, we have also plotted all radio observations of ultracool stars from the literature (see the caption of Figure 5 for references). Our luminosity limits are typically at least two orders of magnitude larger than the most luminous known ultracool stellar flares. Even comparing with the recently detected flare from the T6.5 dwarf 2MASS J1047+21, by far the coolest brown dwarf detected at radio frequencies (Route & Wolszczan 2012), our limits require a radio luminosity a factor of >20 times larger. We furthermore see no evidence for a high degree of circular polarization (common to many, though not all, flares; Berger 2006; Hallinan et al. 2007), and the radio emission from PTF11agg is much more long-lived than these low-mass stellar outbursts (durations typically of only hours).

In addition to stellar flares, binary systems where one member is a compact object (white dwarf, neutron star, or black hole) are known sources of optical and radio outbursts in the Milky Way. Such a system could circumvent two issues with Galactic transients we previously identified. First, the energy release during the accretion process is more than sufficient to power the observed radio flux; Cyg X-3 (Geldzahler et al. 1983), for example, has reached peak radio luminosities in excess of 10^{34} erg s^{-1}. Second, the presence of an accretion disk can alter the optical color of such systems. Accordingly, our previous inference that the quiescent counterpart must lie at $d \gtrsim 90$ kpc would no longer be valid.

We first consider X-ray binaries, where the degenerate primary is a neutron star or black hole. Of particular interest are the subclass of microquasars (Mirabel & Rodríguez 1999), whose powerful radio jets exhibit apparent superluminal motion (and thus imply a relativistic outflow). Due to the lack of a bright quiescent optical counterpart, we consider only low-mass systems where the accretion occurs via Roche-lobe overflow from the nondegenerate secondary (low-mass X-ray binaries, LMXBs).

Black hole LMXBs are typically characterized by well-defined "states": correlations between X-ray spectra, X-ray flux, and radio emission (Remillard & McClintock 2006). Radio emission is observed in a well-defined region of this hardness-intensity phase space (Fender et al. 2004; Falcke et al. 2004). In the so-called low-hard state, thought to correspond to low ($\lesssim$0.01 $L_{\rm Edd}$), radiatively inefficient accretion (Esin et al. 1997), relatively steady radio emission from a jet is observed in most black hole X-ray binary systems. Like PTF11agg, the radio spectrum is flat or inverted ($f_\nu \propto \nu^\beta$, with $\beta \approx 0$–0.5), and circularly unpolarized. However, a reasonably tight correlation

[26] See http://heasarc.gsfc.nasa.gov.
[27] See http://simbad.u-strasbg.fr/simbad.

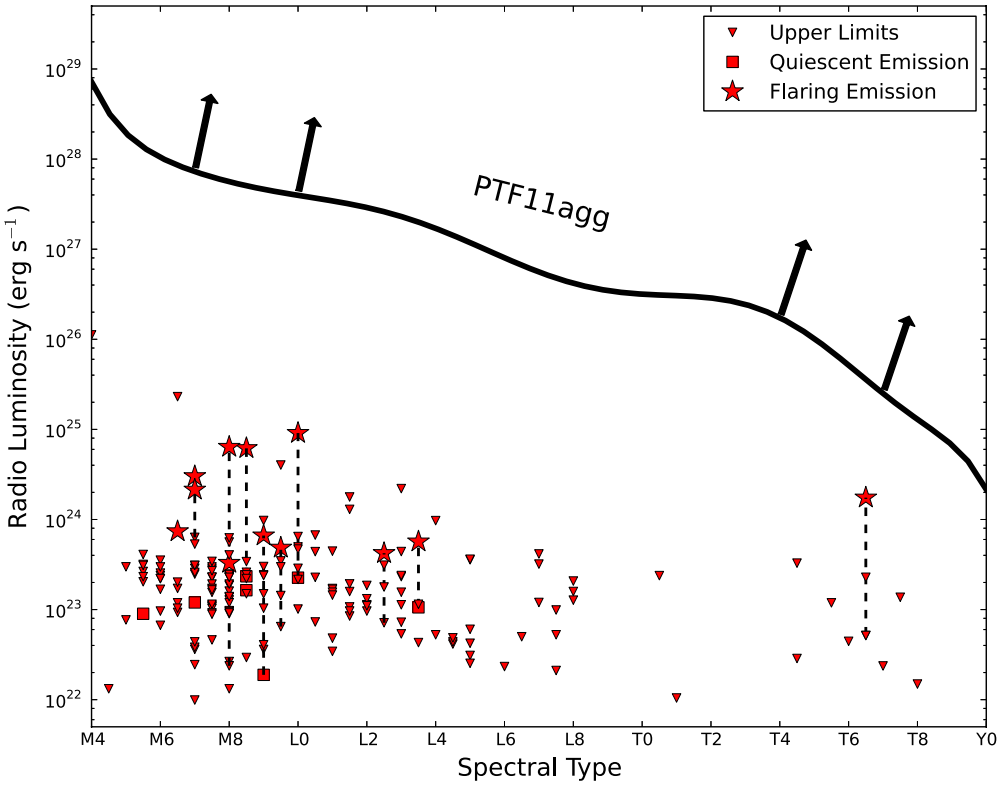

Figure 5. Lower limits on the radio luminosity of PTF11agg (solid black line). For each spectral type, we calculate a minimum "detectability" distance using limits from our NIR imaging (i.e., any source more nearby would have been detected). We then convert this distance to a lower limit on the radio luminosity based on the observed peak flux from PTF11agg. Shown for comparison are radio observations of ultracool stars from the literature (Berger et al. 2001, 2005, 2008a, 2008b, 2009, 2010; Berger 2002, 2006; Antonova et al. 2007; Audard et al. 2007; Burgasser & Putman 2005; Hallinan et al. 2007; Route & Wolszczan 2012; McLean et al. 2012). The inferred luminosity is several orders of magnitude larger than that of any previously observed low-mass star or brown dwarf, either in a quiescent or flaring state.
(A color version of this figure is available in the online journal.)

exists between the radio and X-ray luminosity in the low-hard state (Corbel et al. 2003; Gallo et al. 2003), of the form $f_\nu(\mathrm{radio}) \propto f_\nu(\mathrm{X-ray})^{0.7}$. Using the derived formulation from Gallo et al. (2003) and the observed radio flux, we would expect an X-ray flux of $f_X \approx 2 \times 10^{-12}$ erg cm^{-2} s^{-1} (note that this estimate is entirely independent of the distance to the source). This is more than an order of magnitude above our derived X-ray limits. We further note that while neutron star X-ray binaries do not obey the same radio–X-ray correlation in the hard state, the ratio of X-ray to radio luminosity is even larger in these sources (Muno et al. 2005).

Alternatively, the most luminous radio flares from LMXBs arise as the system transitions through the intermediate state into a bright, quasi-thermal outburst (jet emission at the highest X-ray fluxes appears to be largely suppressed; Fender et al. 2004). Unlike the steady radio jets in the low-hard phase, this state transition in the accretion flow (from radiatively inefficient, advection-dominated to geometrically thin, optically thick; Esin et al. 1997) can sometimes cause the ejection of relativistic material (Mirabel & Rodríguez 1999). While LMXBs in this state do not always follow the same radio–X-ray correlation (Gallo et al. 2003), the radio spectrum from this extended emission becomes optically thin. The X-ray and optical fluxes can rise by several orders of magnitude on a time scale of only a few days during these "X-ray novae," but typically both take many months to return to quiescence (Tanaka & Shibazaki 1996; Charles & Coe 2006).

PTF11agg differs from these X-ray novae in several major respects. Most importantly, to reach the intermediate (and, ultimately, high) state where the radio flare is launched, the compact primary must be accreting material at a substantial fraction of the Eddington limit ($\gtrsim$1%–10%; Esin et al. 1997). As a result, these outbursts have been discovered exclusively by wide-field X-ray or γ-ray satellites. But, for any reasonable Galactic distance scale ($d \lesssim 10$ kpc), our X-ray limits rule out emission at the level of $10^{-5}\,L_{\mathrm{Edd}}$ (for a 1 $M_\odot$ black hole or neutron star). While our X-ray observations were obtained 42 days after the initial optical outburst, this is comparable to the e-folding time of these systems. As it requires $\sim$1 month for the disk mass to accrete onto the neutron star or black hole (the viscous time scale; King & Ritter 1998), this time delay alone cannot account for the many orders of magnitude gap between our limits and the required X-ray luminosity.

In addition to the lack of bright X-ray emission, we note several more characteristics that distinguish PTF11agg from known X-ray nova outbursts: (1) the radio emission at late times remains unresolved, which is difficult to reconcile with relativistic ejecta in our Galaxy; (2) the inverted radio spectrum is inconsistent with the optically thin emission expected at this time; (3) the time scale of the optical decay ($\Delta t \lesssim 2$ days) is significantly shorter than what is observed in X-ray novae ($\tau \approx$ 20–40 days); and (4) the location, well off the Galactic plane ($l = 202^\circ, b = +29^\circ$), is inconsistent with the known population of LMXBs (van Paradijs & White 1995; White & van Paradijs 1996), which have a scale height of $d_z \lesssim 1$ kpc (although several prominent counterexamples are known; Tomsick et al. 1999; Zurita et al. 2000; Hynes et al. 2000; Uemura et al. 2000; Mirabel et al. 2001; Wagner et al. 2001).

Finally, we consider systems with a white dwarf accreting material from a (low-mass) stellar companion or another white dwarf. Short-timescale optical outbursts have been observed from AM CVn systems (a white dwarf accreting H-poor material in a short-period orbit), but never with amplitudes larger than 4 mag (Levitan et al. 2011; Ramsay et al. 2012). Dwarf novae, the analogous phenomenon to X-ray novae in LMXBs (e.g., disk instabilities; Cannizzo 1993), have also previously been mistaken for extragalactic transients (Rau et al. 2007). In fact, the amplitude and duration of the optical outburst from PTF11agg are not unlike the most extreme dwarf novae. But dwarf novae rarely exhibit coincident radio emission (Benz et al. 1996), and the few known examples have outburst durations of only ∼1–2 weeks (Benz et al. 1983; Körding et al. 2008), where the radio emission closely follows the optical evolution.

To summarize, we have examined a variety of known classes of Galactic transients (stellar flares, LMXBs, dwarf novae), and found that PTF11agg does not fit neatly into any of these categories. It should go without saying that it is entirely possible that PTF11agg represents a *new* type of Galactic outburst, characterized by (1) bright, rapidly fading optical emission; (2) a long-lived radio transient; and (3) an extremely subluminous ($M_R \approx 11$ mag for $d = 10$ kpc) quiescent optical counterpart. Given the broad agreement between our observations and the properties of long-duration GRB afterglows (Section 5.1), we do not further explore this possibility here.

4. AN EXTRAGALACTIC ORIGIN: IMPLICATIONS AND COMPARISONS

Having rejected a Galactic origin for PTF11agg, we now consider the possibility that it resides instead at a cosmological distance (i.e., well beyond the Local Group and into the Hubble flow). Assuming the quiescent counterpart is indeed the host galaxy of PTF11agg, we constrain possible redshifts in Section 4.1. Even with these crude constraints, the angular size derived in Section 2.2.3 requires the presence of a relativistic outflow (Section 4.2). Finally, we briefly compare the observed properties with those of known extragalactic sources capable of generating relativistic ejecta in Section 4.3, and quickly settle on a long-duration GRB-like outburst (i.e., the core collapse of a massive star) as the most plausible explanation.

4.1. Redshift Constraints

Assuming the quiescent optical source is related to PTF11agg (Section 2.1.3), we can place an upper limit on its distance based on the absence of redshifted H I absorption along the line of sight (i.e., the Lyman break). Our g' detection implies that redshifted Lyα ($\lambda_{\rm rest} = 1216$ Å) falls at an observed wavelength of $\lambda_{{\rm Ly}\alpha} \lesssim 4800$ Å (i.e., the middle of the g' filter bandpass). This results in an upper limit on the host-galaxy redshift of $z \lesssim 3$.

Alternatively, assuming a modest rest-frame UV luminosity for the host galaxy ($M_{\rm UV} \lesssim -16$ mag, or $L \gtrsim 0.01 L^*$; Reddy et al. 2008), we place a lower limit on the host redshift of $z \gtrsim 0.5$. A similar lower limit is derived if we compare the observed R-band brightness with that of known host galaxies of long-duration GRBs (Jakobsson et al. 2012).

We therefore conclude that the redshift of PTF11agg should fall somewhere in the range $0.5 \lesssim z \lesssim 3.0$.

4.2. Evidence for Relativistic Ejecta

In Section 2.2.3, we derived two independent constraints on the angular diameter of the emitting region from our radio observations: $\Theta > 7\ \mu$as at $\Delta t_{\rm obs} \approx 42$ days, and $\Theta \approx 20\ \mu$as at $\Delta t_{\rm obs} \approx 100$ days. To convert these to constraints on the outflow velocity, we use the redshift limits derived above: $0.5 \lesssim z \lesssim 3.0$ (corresponding to angular-diameter distances of 1.3–1.8 Gpc for a concordance ΛCDM cosmology). Assuming ballistic (i.e., constant velocity) expansion, the angular diameter is then given by

$$\Theta = \frac{\Gamma \beta c t}{d_A (1+z)}, \quad (6)$$

where Γ is the outflow Lorentz factor ($\Gamma \equiv (1-\beta^2)^{-1/2}$), c is the speed of light, t is the time since outburst (in the observer frame), d_A is the angular-diameter distance, and z is the source redshift.

At $z = 0.5$, where our limits on the outflow velocity are the weakest, we find $\Gamma > 1.2$ at $\Delta t_{\rm obs} \approx 42$ days, and $\Gamma \approx 1.3$ at $\Delta t_{\rm obs} \approx 100$ days. These limits vary little over our redshift range of interest, due primarily to the limited evolution of the angular-diameter distance over this range: at $z = 3.0$, we find $\Gamma > 1.6$ at $\Delta t_{\rm obs} \approx 42$ days, and $\Gamma \approx 1.6$ at $\Delta t_{\rm obs} \approx 100$ days.

We therefore conclude that, even at this late time, the ejecta powering the transient emission from PTF11agg are at least transrelativistic. For any more realistic form for the ejecta deceleration (e.g., Blandford & McKee 1976), we infer that PTF11agg was initially at least a modestly relativistic explosion.

4.3. Comparison with Known Relativistic Sources

Only a handful of extragalactic sources are known to produce relativistic ejecta: GRBs, with initial Lorentz factors as least as large as several hundred (Lithwick & Sari 2001), and possibly greater than 1000 (Abdo et al. 2009); AGNs, in particular the subclass of blazars, with Lorentz factors as large as 50 (Lister et al. 2009); and the recently discovered relativistic tidal disruption flares (TDFs; Levan et al. 2011; Bloom et al. 2011; Zauderer et al. 2011; Burrows et al. 2011; Cenko et al. 2012), with initial Lorentz factors ∼10 (Metzger et al. 2012; Berger et al. 2012b; van Velzen et al. 2011). Though with only one or two examples to date, the known relativistic TDFs do not appear to vary in the optical on time scales as short as those of PTF11agg, where $\delta t \ll 1$ day. Furthermore, the SEDs of these sources are dominated by the soft X-ray (∼1–10 keV) bandpass, with peak isotropic luminosities as large as $L_X \approx 10^{48}$ erg s^{-1}. Even at $z = 3$, our X-ray limits (Section 2.3.2) imply $L_X < 6 \times 10^{45}$ erg s^{-1}.

Blazars, however, are known to vary in the optical on short time scales ($\delta t < 1$ day), and have previously been mistaken for optically discovered GRB afterglows (Vanden Berk et al. 2002; Gal-Yam et al. 2002). But significant ($m_p \gtrsim 10\%$) interstellar scintillation is observed only very rarely in blazars ($\lesssim$1% of the population; Lovell et al. 2008). More importantly, the degree of optical variability observed from PTF11agg, in particular the amplitude from peak to quiescence ($\Delta R \gtrsim 8$ mag in $\Delta t \approx 1$ month), makes this source unlikely to belong to any known AGN class (MacLeod et al. 2012).

On the other hand, a long-duration GRB can naturally accommodate all of the observed properties of PTF11agg. We find that the standard GRB afterglow fireball model can accurately reproduce the observed optical and radio light curves (Section 5.1). The small initial size of the ejecta explains the observed interstellar scintillation, though this should be quenched as the blast wave expands relativistically (usually on a time scale of weeks to months). The faint, blue quiescent optical counterpart is consistent with the long-duration GRB

host-galaxy brightness distribution for $z \gtrsim 0.5$ (Jakobsson et al. 2012). We therefore conclude that the most likely explanation for PTF11agg is a long-duration GRB-like (i.e., massive star core collapse) explosion, the first time such an event has been discovered at cosmological distances absent a high-energy trigger.

5. PTF11agg AS A GRB: UNTRIGGERED, ORPHAN, OR DIRTY FIREBALL?

Broadly speaking, there are three reasons why a distant, relativistic outburst may lack detected prompt high-energy emission. The null hypothesis is a lack of sky coverage (i.e., an "untriggered" GRB), as the more sensitive high-energy satellites (*Swift* and *Fermi*) have only a ∼60% combined likelihood of detecting any given event (Section 2.3.1). The limiting γ-ray fluence from the only all-sky satellite available (the IPN) corresponds to an isotropic γ-ray energy release of $E_{\gamma,\rm iso} = (2\text{–}200) \times 10^{50}$ erg from $z = 0.5\text{–}3.0$. These values are not sufficiently low to rule out typical cosmological long-duration GRBs (Butler et al. 2007), let alone the class of subluminous (e.g., GRB 980425/SN 1998bw-like) events uncovered in relatively nearby galaxies (Soderberg et al. 2006a; Cobb et al. 2006; Guetta & Della Valle 2007). Without any additional information, the simplest explanation is that PTF11agg is an otherwise normal but untriggered long-duration GRB.

There exist other, more intriguing, possibilities, however. The second possible explanation for a GRB-like explosion absent any high-energy signature is a viewing-angle effect. Due to their high degree of collimation (Sari et al. 1999; Rhoads 1999), the prompt emission from most GRBs is beamed away from our line of sight. However, the long-lived afterglow emission may nonetheless be visible, either if the region generating the afterglow is less beamed than the γ-ray emitting material (i.e., an on-axis orphan afterglow; Nakar & Piran 2003), or if, as expected, the outflow spreads laterally at late times and illuminates an increasing fraction of the sky (i.e., an off-axis orphan afterglow; Rhoads 1997; Perna & Loeb 1998; Nakar et al. 2002). The discovery of a *bona fide* orphan afterglow would provide robust constraints on the GRB beaming fraction, still a large source of uncertainty in calculations of the true energy release and the all-sky rate of GRBs.

Finally, a source may lack detectable high-energy emission altogether, either because no high-energy photons were produced, or such emission may be unable to escape to distant observers due to some internal suppression mechanism. It has long been noted (e.g., Piran 2004 and references therein) that the baryon composition of the relativistic jet in the fireball model must be very finely tuned in order to generate any detectable prompt high-energy emission (the so-called "baryon loading problem"). Without any baryons in the ejecta, the internal shocks thought to power the prompt emission will not form.[28] But with too large a baryon fraction, the jet will not accelerate to a sufficiently high initial Lorentz factor ($\Gamma_0 \gtrsim 20$), inhibiting any high-energy emission via e^-–e^+ pair production (Huang et al. 2002; Ghirlanda et al. 2012). Such explosions, dubbed "dirty fireballs," have long been predicted (Dermer et al. 2000; Huang et al. 2002; Rhoads 2003) to occur as a result of a modest baryon loading of the jet; a proton content as small as $M \gtrsim 10^{-4}\,M_\odot$ will lower the initial Lorentz factor sufficiently ($\Gamma_0 \approx E_{\rm KE}/Mc^2$), yet can still produce the observed broadband afterglow. Distinguishing between a source that produces no high-energy emission whatsoever and one in which these photons are unable to escape is clearly challenging—for the remainder of this work we shall refer to such objects generically as dirty fireballs or afterglows lacking prompt high-energy emission.

Here we attempt to discriminate between these competing hypotheses through two different means. First, we distinguish between on-axis and off-axis models by comparing the observed optical and radio emission with analytic and numerical predictions for GRB afterglow light curves in the fireball model (Section 5.1). Second, we calculate the rate of PTF11agg-like outbursts to determine if it is consistent with the all-sky (on-axis) GRB event rate (Section 5.2).

5.1. PTF11agg and the Fireball Model

In the standard GRB afterglow fireball model (see, e.g., Piran 2004 for a review), relativistic ejecta with (kinetic) energy $E_{\rm KE}$ sweep up material in the circumburst medium, forming a collisionless shock and accelerating electrons to a power-law distribution of energies with exponent p and minimum Lorentz factor $\gamma_{\rm m}$. It is assumed that a constant fraction of the total post-shock energy density is partitioned to the electrons (ϵ_e) and the magnetic field (ϵ_B). These accelerated electrons then emit synchrotron radiation, powering the long-lived X-ray, optical, and radio afterglow.

The observed afterglow spectrum depends on the relative ordering of three critical frequencies: the frequency where self-absorption becomes important ($\nu_{\rm a}$), the characteristic frequency of the emission ($\nu_{\rm m}$), and the frequency above which electrons are able to cool efficiently through radiation ($\nu_{\rm c}$). We shall assume that all our observations occur in the "slow" cooling regime ($\nu_{\rm m} < \nu_{\rm c}$), and that the self-absorption frequency falls below the frequency range probed by our observations ($\nu_{\rm a} < 10^9$ Hz).

The light curve produced by such emission depends on the radial profile of the circumburst medium into which the shock is expanding. The simplest circumburst medium to consider is one in which the density is constant ($\rho \propto r^0$). This scenario is also referred to as an interstellar medium (ISM; Sari et al. 1998), and is parameterized in terms of the particle number density n_0, where $\rho = m_p n_0$ g cm^{-3}.

Long-duration GRBs, however, have been conclusively linked to the deaths of massive stars (e.g., Woosley & Bloom 2006). In the late stages of evolution, massive Wolf–Rayet stars are stripped of their outer H and (possibly) He envelopes in a wind, leaving behind a signature $\rho \propto r^{-2}$ density profile that should be discernible in the afterglow light curve. Wind-like environments (Chevalier & Li 2000) are parameterized in terms of A_*, where $\rho = 5 \times 10^{11} A_* r^{-2}$ g cm^{-3}.

Finally, we note that the hydrodynamical evolution also depends on the geometry of the outflow. GRBs are now widely believed to be aspherical explosions (Rhoads 1999; Sari et al. 1999), biconical jets with half-opening angle $\theta_{\rm j}$. At early times, the jet emission is collimated into a narrow cone ($\theta_{\rm eff} \approx \Gamma^{-1} \ll \theta_{\rm j}$, where Γ is the Lorentz factor of the expanding shock) due to relativistic beaming. As the shock slows, however, simple analytic solutions suggest that lateral spreading of the jet becomes important, and on-axis observers eventually "miss" emission from wider angles. This hydrodynamic transition manifests itself as an achromatic steepening in the afterglow light curve (the "jet break"), with an expected post-break decay proportional to t^{-p}. While more recent numerical simulations have suggested

[28] An alternative possibility is that the prompt emission is generated by magnetic dissipation in a Poynting-flux-dominated outflow (see, e.g., Lyutikov & Blandford 2003).

a more complex picture of the jet-break phenomenon (Zhang & MacFadyen 2009; van Eerten et al. 2010; Granot & Piran 2012), the assumption of a general light-curve steepening around the time when $\Gamma = 1/\theta_j$ remains largely valid.

At $\Delta t \approx 0.2$ days (the approximate time of discovery), we expect the optical bandpass to fall below the cooling frequency (i.e., $\nu_{opt} < \nu_c$). If we also assume that these early optical data occur before any jet break (see below), the observed temporal decay index ($\alpha_{opt} = 1.66 \pm 0.35$) can be translated directly into the electron spectral index p. For a constant-density medium, we find $p = 3.21 \pm 0.47$, while for a wind-like environment, we infer $p = 2.55 \pm 0.46$. Electron spectral indices derived from previous observations of long-duration GRBs (Shen et al. 2006; Starling et al. 2008; Curran et al. 2010) fall in the range ~2–3, so the large uncertainty makes it difficult to distinguish between the competing density profiles solely on this basis.

While the radio emission is relatively variable at $\Delta t \gtrsim 40$ days, the approximate radio spectral index, $\beta_{radio} \approx 0.3$, implies that the peak synchrotron frequency ν_m is not well below the radio at this time (or else we would expect $\beta_{radio} \approx -1$). Conservatively, we assume $\nu_m(\Delta t = 40\,\mathrm{days}) \gtrsim 10$ GHz, and $f_{\nu_m}(\Delta t = 40\,\mathrm{days}) \gtrsim 300\,\mu$Jy. For a wind-like medium, $\nu_m \propto t^{-3/2}$ and $f_{\nu_m} \propto t^{-1/2}$. Extrapolating back to the time of optical discovery, we conclude $\nu_m(\Delta t = 0.2\,\mathrm{days}) \gtrsim 3 \times 10^{13}$ Hz, and $f_{\nu_m}(\Delta t = 0.2\,\mathrm{days}) \gtrsim 4 \times 10^3\,\mu$Jy. For $\nu_m < \nu < \nu_c$, $f_\nu \propto \nu^{(1-p)/2} \approx \nu^{-0.77}$. Thus, we find that the inferred optical (R-band) flux at discovery, $f_\nu \gtrsim 500\,\mu$Jy, is a factor of ~3 larger than our observations at this time. For a constant-density environment, the peak flux is constant in time, and so a similar analysis yields a self-consistent result. We therefore do not consider a wind-like medium any further.

Using these general constraints, we have used the software described by van Eerten et al. (2012) to fit the observed optical and radio light curves to afterglow models calculated from high-resolution two-dimensional relativistic hydrodynamical jet simulations. In all cases, we have assumed a constant-density circumstellar medium and adopted a fiducial redshift of 1. We find that a relatively wide set of parameters is able to reproduce the observations,[29] largely consistent with values derived from previous GRB afterglow modeling (Panaitescu & Kumar 2001a, 2001b; Yost et al. 2003), although with a somewhat smaller circumburst density ($n_0 \lesssim 0.1$ cm^{-3}). The best-fit model, assuming the observer is oriented directly along the jet axis (i.e., $\theta_{obs} = 0$), is plotted in Figure 6 ($E_{KE} = 3 \times 10^{52}$ erg, $\theta_j = 0.50$ rad, $n_0 = 1 \times 10^{-3}$ cm^{-3}, $\epsilon_e = 0.1$, $\epsilon_B = 0.1$, and $p = 2.9$). Repeating a similar analysis with the software described by Yost et al. (2003) yields qualitatively similar results. The general agreement between the fireball model and our optical and radio observations supports our conclusion that PTF11agg is most likely a distant, relativistic explosion like other long-duration GRBs.

One concern regarding the $z = 1$ models is the implied angular size of the source (Θ). In the best-fit on-axis model, we find that the outflow has an angular size $\Theta \approx 40$ mas at $\Delta t = 40$ days. This is somewhat larger than the value inferred from our scintillation analysis, but within a factor of two. However, many of the other $z = 1$ models that provide a reasonable fit to the data are likely to be too spatially extended to scintillate strongly at $\Delta t \approx 100$ days. One potential solution may be a more distant origin; due to cosmological time dilation, an observer-frame time of $\Delta t = 100$ days would correspond to only 25 rest-frame days post-explosion at $z = 3$, half the expansion time as inferred at $z = 1$. Given the large spread in acceptable models, however, we do not explore this possibility further here.

Next we consider limits on the opening angle and observer orientation from the observed optical and radio emission. After the jet break, the peak synchrotron flux declines linearly with time (in a constant-density environment). Thus, if the jet break occurred well before the first radio observations, the large radio flux would be difficult to reconcile with our early optical observations. We consider it likely, then, that $t_j \gtrsim 40$ days. These conclusions are largely confirmed by our numerical models, where we find that the opening angle is only weakly constrained to be $\theta_j \gtrsim 0.15$ rad.

In addition to cases where the observer is oriented directly along the jet axis (i.e., $\theta_{obs} = 0$), we also have considered more general geometries, where the observer may be oriented off-axis, either within (i.e., $\theta_{obs} < \theta_j$) or outside ($\theta_{obs} > \theta_j$) the jet opening angle. For simplicity, we consider only "top-hat" jet geometries, where the jet Lorentz factor is given by a step function. For $\theta_{obs} > \theta_j$, observers will see rising emission until approximately the time of the jet break, after which the decay will resemble the on-axis case. For observers off-axis but within the jet opening angle, the modifications to the on-axis afterglow light curves will be more subtle (Granot et al. 2002; Zhang & MacFadyen 2009; van Eerten et al. 2010).

The arguments used above to infer $t_j \gtrsim 40$ days necessarily require that the observer cannot be well outside the jet opening angle (or else we would expect to see post jet-break decay). This result is borne out by our numerical modeling, where geometries with $\theta_{obs} > \theta_j$ are unable to accurately reproduce the observed light curves. Allowing the observer orientation to vary as a free parameter, the best-fit afterglow model is plotted as a dashed line in Figure 6 ($E_{KE} = 9 \times 10^{52}$ erg, $\theta_j = 0.20$ rad, $\theta_{obs} = 0.19$ rad, $n_0 = 1 \times 10^{-3}$ cm^{-3}, $\epsilon_e = 0.04$, $\epsilon_B = 0.2$, and $p = 3.0$).

Finally, we can derive a lower limit on the distance to PTF11agg based only on the observed radio evolution. The radio spectrum at $\Delta t = 67$ days, $f_\nu \propto \nu^\beta$, with $\beta \approx 0.3$, is inconsistent with Sedov–Taylor blast-wave evolution. In other words, the outgoing shock wave has not transitioned to non-relativistic expansion at this point in time. The nonrelativistic transition will occur at a time (Wygoda et al. 2011)

$$t_{nr} = 1100 \left(\frac{E_{KE}}{10^{53}\,\mathrm{erg}}\right) \left(\frac{n_0}{1\,\mathrm{cm}^{-3}}\right) \mathrm{days}. \quad (7)$$

Even neglecting our previous finding of a low circumburst density, we infer a sizeable lower limit on the blast-wave kinetic energy: $E_{KE} \gtrsim 10^{50}$ erg. Integrating over the observed 8 GHz radio light curve, we measure a fluence of $S_{rad} = 2 \times 10^{-10}$ erg cm^{-2}. For a typical cosmological distance ($z = 1$, or $d_L = 2 \times 10^{28}$ cm), this corresponds to a radiated energy of $E_{rad} = 3 \times 10^{47}$ erg, a typical radiative efficiency for a GRB. But for a Galactic outburst, the radiated energy would be many orders of magnitude smaller ($E_{rad} = 6 \times 10^{35}$ erg at $d = 10$ kpc). Unless the radiative efficiency was incredibly small, we once again conclude that PTF11agg must lie at a cosmological distance.

5.2. The Rate of PTF11agg-like Events

Our objective in this section is to estimate the number of GRB optical afterglows discovered by chance (i.e., not as a result of

[29] In all cases the predicted X-ray flux is well below the XRT limit (Section 2.3.2), so we have not included this point in our fitting.

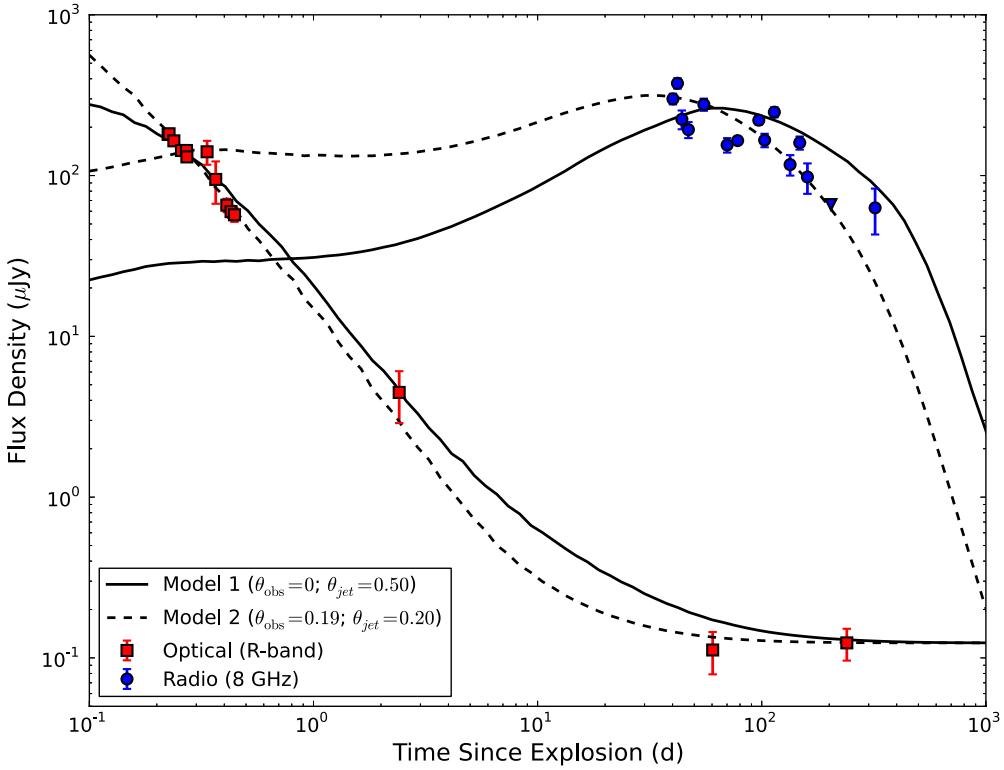

Figure 6. The solid line shows the best-fit afterglow model (van Eerten et al. 2012) when the relativistic jet is oriented directly along the line of sight to the observer (i.e., $\theta_{obs} = 0$). The dashed curve displays the best-fit model when the viewing angle is allowed to vary freely. Given the relatively sparse data set (in particular the lack of X-ray observations), a wide variety of models are able to reproduce the observed optical and radio emission. However, we find it impossible to reproduce the observed emission when the viewing angle is outside the cone of the jet (i.e., $\theta_{obs} > \theta_j$). We therefore consider it unlikely that viewing angle alone can account for the lack of high-energy emission from PTF11agg.

(A color version of this figure is available in the online journal.)

deliberate follow-up observations of a high-energy trigger) by PTF. If the likelihood of chance detection of an untriggered afterglow with PTF is significant, we will conclude that the rate of PTF11agg-like events is consistent with the rate of normal (i.e., on-axis) long-duration GRBs. If this probability is small, then we can use these calculations to place lower limits on the observed frequency of PTF11agg-like outbursts (in units of the GRB rate). Given the relatively complex nature of PTF scheduling (Law et al. 2009), we have conducted a series of Monte Carlo simulations to this end.

PTF began full operations on about 2009 April 1. We have retrieved a listing of all images obtained beginning at this time through 2012 December 31, or over a period of 45 months. We removed fields at Galactic latitude $|b| < 20^\circ$ (due to the large foreground extinction).[30] The resulting sample includes 129,206 pointings, each covering an area of 7.2 deg^2. The sample comprises 1940 unique fields, each imaged an average of 67 times.

Since its launch, the *Swift* BAT[31] detects GRBs at a rate of $\approx$90 yr^{-1}. The field-of-view of the BAT is $\sim$2 sr, and the instrument has a duty cycle of $\sim$90%. Thus, the all-sky rate for events at the BAT threshold is $\sim$630 yr^{-1}. Over the 3.75 yr period of interest, the total number of all-sky GRBs is $\sim$2360. We note that this is an upper limit to the long-duration GRB rate, as we have included short-duration GRBs in this sample as well.

For each trial, we create a mock catalog of 2360 GRBs. Each GRB is randomly assigned a trigger time t_0 (uniformly distributed between 2009 April 1 and 2012 December 31) and spatial coordinates α, δ (isotropically distributed on the sky). To estimate the duration over which the optical afterglow would be detectable by PTF, we utilize the sample of 29 long-duration afterglows from the Palomar 60 inch (P60) *Swift* afterglow catalog (Cenko et al. 2009). These events were selected solely on the basis of visibility to the Palomar Observatory, so they should represent an unbiased sample of the *Swift* afterglow brightness distribution. For each event in the P60-*Swift* sample, we have calculated the amount of time following the high-energy trigger that the afterglow is brighter than $R = 20$ mag. These values range from <204 s (GRB 050721) to 1.2 days (GRB 050820A). Each mock GRB is randomly assigned one of the 29 actual "visibility windows" from this sample.[32]

For each mock GRB, we then determine if the event occurred within the 7.2 deg^2 footprint of any individual PTF image, and, if so, if the time of observation occurred within the necessary window during which the afterglow was brighter than 20 mag. The number of afterglows detected in each trial (N_{GRB}), together with the number of individual frames on which each detected afterglow was brighter than the P48 sensitivity limit (N_{Det}), were then recorded. The results of 1000 individual runs (i.e., different randomly selected groups of 2360 GRBs) constitute a sufficiently large sample to evaluate the likelihood

[30] Given that the primary objective of PTF is the discovery of extragalactic transients, this represents less than 10% of the total number of observations.

[31] See http://swift.gsfc.nasa.gov/docs/swift/archive/grb_table.

[32] For GRBs without any detected optical afterglow (e.g., "dark" bursts), we use the earliest non-detection below our sensitivity threshold for the visibility window. If anything, this would bias us to overestimate the expected number of untriggered GRB afterglow detections by PTF.

Table 3
PTF GRB Simulation Results

N	$N_{\rm Det}$	$N_{\rm Obs}$
1	1311	11376
2	1583	40101
3	228	5889
4	118	825
5	30	693
6	31	305
7	6	189
8	4	113
9	3	54
>10	26	426

of serendipitous detection of long-duration GRB afterglows with PTF.

In the 1000 trials conducted, at least one GRB afterglow was detected (i.e., $N_{\rm GRB} \geqslant 1$) in 970 instances. Thus, the probability of detecting at least one on-axis afterglow over the course of the first two years of PTF is quite high, $P(N_{\rm GRB} \geqslant 1) = 97\%$. The expectation value for the number of afterglows detected is $\lambda = 3.3$. The distribution of the number of afterglows detected in our 1000 trials is reasonably well described by Poisson statistics (Figure 7). In this respect, then, PTF11agg appears to be consistent with a normal on-axis GRB.

However, the field in which PTF11agg was identified (the Beehive cluster) is atypical amongst PTF pointings. Most fields are only observed two or three times per night (multiple images are used to identify solar system objects). But the Beehive cluster is a "high-cadence" field, observed many times ($\gtrsim$10) per night during its observing season. Instead of calculating the rate of afterglow detections over the entire survey (i.e., $N_{\rm GRB}$), a more appropriate comparison would limit the scope to similar high-cadence fields.

We therefore consider on how many individual images each of the 3340 "detected" GRB afterglows (in our 1000 trials) were above the P48 limiting magnitude (i.e., $N_{\rm Det}$). This is illustrated in Table 3. The vast majority of the afterglows are detected on only one or two images (87%). In fact, in our 1000 trials, an optical afterglow was detected on at least 10 individual images only 11 times (i.e., $P(N_{\rm Det} \geqslant 10) = 2.6\%$). PTF11agg was detected 11 times on 2011 January 30 with $R < 20$ mag.

We can understand this result analytically in the following manner. In the case where the integration time (δt) is much smaller than the period over which a transient is visible (τ), the number of detectable events at any given time will be

$$q = \frac{\Omega \mathcal{N} \tau}{4\pi}, \tag{8}$$

where Ω is the field of view (in steradian) and $\mathcal{N}$ is the all-sky event rate. For long-duration GRB optical afterglows, serendipitous detection by PTF will be dominated by the $\sim$10% of events that remain brighter than $R < 20$ mag for $\tau \approx 1$ day (certainly this is true for those afterglows with $N_{\rm Det} > 3$). Thus, for the PTF project, $\Omega/4\pi = 1.7 \times 10^{-4}$ sr (7.2 deg^2), and adopting $\mathcal{N} \approx 0.1 \times 630$ yr^{-1} and $\tau \approx 2.7 \times 10^{-3}$ (1 day), we find $q \approx 3.0 \times 10^{-5}$ events per field.

The expected number of detected events, λ, will then be $q N_{\rm Obs}$, where $N_{\rm Obs}$ is the number of (independent) measurement epochs. Over the two-year period of interest, the number of individual P48 images obtained is $N_{\rm Obs}({\rm all}) = 1.3 \times 10^5$. Thus, we predict $\lambda \approx 3.7$, in good agreement with the results of our Monte Carlo simulations.

Conversely, we can calculate the relative frequency of high-cadence ($N_{\rm Obs}[>10]$) observations in our two-year PTF sample by measuring how often each field was observed on a nightly basis. The results of this analysis are shown in the far-right column of Table 3. As is evident, high-cadence observations with $N_{\rm Obs}(>10)$ (i.e., more than 10 observations of a field obtained in a single night) occur with a frequency of 1% when compared with regular-cadence fields ($N_{\rm Obs}[1] + N_{\rm Obs}[2]$).

From this analysis, we conclude that the rate of PTF11agg-like events is inconsistent with the rate of long-duration GRBs with 97.4% confidence. Admittedly, a number of assumptions went into this analysis, and one should always be careful with results drawn from such an a posteriori analysis. But, independent of the exact likelihood, we conclude that the probability of untriggered afterglow detection in a high-cadence PTF field is small. Either we have been quite lucky, or we may have uncovered a new, more common class of distant, relativistic outbursts lacking entirely in high-energy emission.

It is crucial to verify, however, that our inferred rate does not violate any other limits on short-timescale transients, either from PTF itself, or from previous optical and radio surveys. As highlighted above, low-cadence fields are observed significantly more frequently with PTF than high-cadence fields like the Beehive. Thus, any short-timescale ($\Delta t \lesssim 1$ day) transient should be detected in many more $N_{\rm Obs}(1)$ and $N_{\rm Obs}(2)$ fields than high-cadence fields. In the case of PTF11agg, repeating the above Monte Carlo simulations for a transient population with five times the GRB event rate (but the same optical brightness distribution), we find an expected number of detected sources of $\lambda = 16.7$ in all fields. At first glance, the fact that we have not discovered such a population of sources would seem to favor the untriggered GRB scenario.

Here it is important to distinguish between transient detection, by which we mean a source is above the P48 sensitivity limit on a given image, and discovery, where a transient is flagged as astrophysically interesting (by software or human beings; Bloom et al. 2012). Because of the large number of uncataloged asteroids near the PTF limit, our software requires at least two detections at a given location to flag a source as a *bona fide* transient (e.g., to "discover" the source). Thus, any PTF11agg-like outburst with only a single detection ($N_{\rm Det} = 1$) will never be discovered by our survey. Likewise, there may be subtle biases limiting our capability to identify and/or conduct follow-up observations of similar short-timescale transients with only a few detections.

Whether these discovery biases are sufficient to account for the lack of similar sources in our low-cadence fields with PTF remains to be seen. We have attempted to search through all PTF discoveries that were detected only on a single night (independent of $N_{\rm Det}$),[33] but have yet to uncover any additional viable candidates. Ultimately, future wide-field, high-cadence optical surveys may be required to resolve this issue.

Finally, we compare our derived rate of PTF11agg-like events with previous searches for orphan optical (Vanden Berk et al. 2002; Becker et al. 2004; Rykoff et al. 2005; Rau et al. 2006, 2008; Malacrino et al. 2007) and radio (Levinson et al. 2002; Berger et al. 2003; Gal-Yam et al. 2006; Soderberg et al. 2006b) afterglows, to verify that our results are consistent with these limits. The tightest constraints on the rate of relativistic outbursts come from radio surveys, where Gal-Yam et al.

[33] We cannot avoid the requirement of at least two detections, however. Otherwise we would be completely swamped with asteroids, which are detected at a rate of thousands per night.

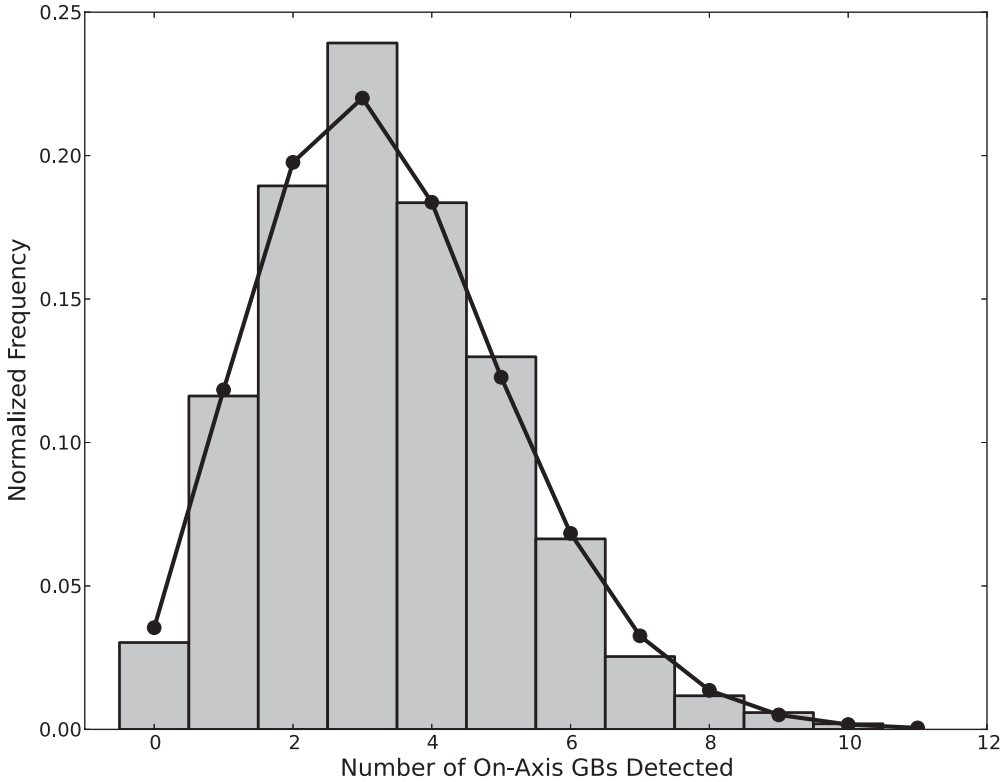

Figure 7. Normalized histogram of the number of serendipitous detections of normal on-axis GRB afterglows by PTF in our 1000 Monte Carlo trials. The distribution is reasonably well described by a Poisson function with $\lambda = 3.3$ (solid black line).

(2006) derive a limit on the all-sky volumetric rate of GRB-like explosions of $\dot{N} < 10^3$ events Gpc^{-3} yr^{-1}. Even assuming an all-sky GRB rate as large (Guetta & Della Valle 2007) as 100 Gpc^{-3} yr^{-1} (more recent estimates suggest a significantly smaller value; Butler et al. 2010), a population of PTF11agg-like events occurring at a rate of $\sim$5 times that of normal GRBs is consistent with these results. Our derived rate is therefore orders of magnitude lower than the all-sky rate of Type Ibc supernovae ($\dot{N} = 2.6 \times 10^4$ Gpc^{-3} yr^{-1}; Li et al. 2011). It may approach the rate of low-luminosity GRBs (Soderberg et al. 2006a; Cobb et al. 2006; Guetta & Della Valle 2007), although this depends both on the assumed beaming correction and the true GRB rate.

6. SUMMARY AND CONCLUSIONS

To summarize our results, we report here the discovery of PTF11agg, a rapidly fading optical transient with a long-lived, scintillating radio counterpart. Together with the observed optical and radio light curves, the detection of a faint, blue quiescent counterpart at the location of PTF11agg indicates that the transient likely originated in the distant universe. Using our measurements of the source size derived from the radio observations, we infer that PTF11agg must be powered by a relativistic outflow. These properties are all consistent with the population of long-duration GRB afterglows, marking the first time such an event has been discovered at cosmological distances without a high-energy trigger.

Searching various high-energy satellites, we find no potential γ-ray counterpart for PTF11agg. We therefore consider three possible explanations that can simultaneously account for a GRB-like explosion without any associated prompt high-energy emission: an untriggered GRB, an orphan afterglow, and a dirty fireball.

Using the all-sky rate of GRBs discovered by the *Swift* satellite, together with a measurement of their observed optical brightness distribution, we have calculated the likelihood of serendipitous untriggered GRB afterglow detection by PTF (2009 April–2012 December). Surprisingly, we found that the a posteriori probability of untriggered GRB afterglow detection in a high-cadence field like the one where PTF11agg was found (11 observations on a single night) is only 2.6%. While we cannot entirely rule out our null hypothesis that PTF11agg is an untriggered GRB, this probability is sufficiently low that we consider alternative interpretations as well.

The afterglow emission from an orphan GRB will rise in flux at early times, as more and more of the jet becomes visible due to relativistic beaming effects. Using both analytic and numerical formulations, we are unable to reproduce the observed PTF11agg light curves unless the observer viewing angle is within the opening angle of the jet. While these models assume a relatively simple jet structure, the requirement of rising afterglow emission at early times is a robust prediction for all off-axis models.

A more intriguing possibility is that PTF11agg may represent a new class of relativistic outbursts with little or no corresponding high-energy emission. In much the same way that SN 2009bb (Soderberg et al. 2010) demonstrated that the more nearby, sub-luminous class of GRBs may generate relativistic ejecta yet lack high-energy emission, PTF11agg may play an analogous role for the more energetic, cosmologically distant sample of long-duration GRBs. Dirty fireballs (i.e., a baryon-loaded jet) are one possible explanation (Chakraborti & Ray 2011), though alternative possibilities surely exist as well.

In this picture, the inferred rate of PTF11agg-like events must be four times higher (90% confidence) than the rate of on-axis long-duration GRBs. When combined with traditional

core-collapse supernovae and long-duration GRBs, these objects would enable a more complete census of the deaths of massive stars, and also provide a probe of the location of massive-star formation in distant galaxies without the need for a high-energy satellite trigger.

Regardless of its ultimate origin, we expect such sources to be discovered in large numbers by ongoing and future wide-field, high-cadence optical surveys such as the Catalina Real-Time Transient Survey (Drake et al. 2009), PTF, Pan-STARRS (Kaiser et al. 2010), and the Large Synoptic Survey Telescope (Ivezic et al. 2008). Furthermore, the discovery of PTF11agg bodes well for optical surveys in the future era of gravitational wave astronomy, as the electromagnetic counterparts of gravitational wave sources should exhibit largely similar observational signatures (though they are also expected to be associated with more nearby galaxies; Nakar & Piran 2011; Metzger & Berger 2012).

We thank David Levitan and Kunal Mooley for obtaining observations used in this work, and John Tomsick for valuable comments on the manuscript. We are grateful to the following IPN team members for sharing their data: K. Hurley, I. G. Mitrofanov, D. Golovin, M. L. Litvak, A. B. Sanin, W. Boynton, C. Fellows, K. Harshman, R. Starr, S. Golenetskii, R. Aptekar, E. Mazets, V. Pal'shin, D. Frederiks, D. Svinkin, A. von Kienlin, X. Zhang, K. Yamaoka, T. Takahashi, M. Ohno, Y. Hanabata, Y. Fukazawa, M. Tashiro, Y. Terada, T. Murakami, K. Makishima, T. Cline, S. Barthelmy, J. Cummings, N. Gehrels, H. Krimm, D. Palmer, J. Goldsten, V. Connaughton, M. S. Briggs, and C. Meegan.

A.V.F. and his group acknowledge generous financial assistance from Gary and Cynthia Bengier, the Richard and Rhoda Goldman Fund, the Christopher R. Redlich Fund, NASA/*Swift* grants NNX10AI21G and NNX12AD73G, the TABASGO Foundation, and NSF grant AST-1211916. A.C. acknowledges support from LIGO, which was constructed by the California Institute of Technology and the Massachusetts Institute of Technology with funding from the NSF and operates under cooperative agreement PHY-0757058. D.A.P. is supported by NASA through Hubble Fellowship grant HST-HF-51296.01-A awarded by the Space Telescope Science Institute, which is operated by the Association of Universities for Research in Astronomy, Inc., for NASA, under contract NAS 5-26555. Research by A.G.Y. and his team is supported by grants from the ISF, BSF, GIF, the EU/FP7 via an ERC grant, and a Kimmel Award. P.J.G. acknowledges support from Caltech during his 2011 sabbatical stay. E.O.O. is incumbent of the Arye Dissentshik career development chair and is grateful to support by a grant from the Israeli Ministry of Science. A.A.M. is supported by the NSF Graduate Research Fellowship Program. J.S.B. acknowledges NSF grant CDI-0941742. D.P. is grateful for the AXA research fund. A.S. is supported by a Minerva Fellowship. M.M.K. acknowledges generous support from the Hubble Fellowship and Carnegie-Princeton Fellowship.

Observations were obtained with the Samuel Oschin telescope and the Hale telescope at Palomar Observatory as part of the Palomar Transient Factory project, a scientific collaboration between the California Institute of Technology, Columbia University, Las Cumbres Observatory, the Lawrence Berkeley National Laboratory, the National Energy Research Scientific Computing Center, the University of Oxford, and the Weizmann Institute of Science. The National Energy Research Scientific Computing Center, supported by the Office of Science of the U.S. Department of Energy, provided staff, computational resources, and data storage for this project. Support for CARMA construction was derived from the Gordon and Betty Moore Foundation, the Kenneth T. and Eileen L. Norris Foundation, the James S. McDonnell Foundation, the Associates of the California Institute of Technology, the University of Chicago, the states of California, Illinois, and Maryland, and the NSF. Ongoing CARMA development and operations are supported by the NSF under a cooperative agreement, and by the CARMA partner universities. Some of the data presented herein were obtained at the W. M. Keck Observatory, which is operated as a scientific partnership among the California Institute of Technology, the University of California and NASA; the Observatory was made possible by the generous financial support of the W. M. Keck Foundation. PAIRITEL is operated by the Smithsonian Astrophysical Observatory (SAO) and was made possible by a grant from the Harvard University Milton Fund, a camera loan from the University of Virginia, and continued support of the SAO and UC Berkeley. The PAIRITEL project is further supported by NASA/*Swift* Guest Investigator grant NNX08AN84G. This work made use of data supplied by the UK *Swift* Science Data Centre at the University of Leicester. It also made use of the NASA/IPAC Extragalactic Database (NED), which is operated by the Jet Propulsion Laboratory, California Institute of Technology, under contract with NASA. In addition, we have utilized the SIMBAD database, operated at CDS, Strasbourg, France.

Facilities: PO:1.2m (PTF), Hale (WIRC), Keck:I (LRIS), Magellan:Baade (IMACS), FLWO:2MASS (PAIRITEL), VLA, CARMA, Fermi (GBM), Swift (BAT, XRT)

REFERENCES

Abdo, A. A., Ackermann, M., Ajello, M., et al. 2009, ApJL, 706, L138
Agüeros, M. A., Covey, K. R., Lemonias, J. J., et al. 2011, ApJ, 740, 110
Aihara, H., Allende Prieto, C., An, D., et al. 2011, ApJS, 193, 29
Antonova, A., Doyle, J. G., Hallinan, G., Golden, A., & Koen, C. 2007, A&A, 472, 257
Audard, M., Osten, R. A., Brown, A., et al. 2007, A&A, 471, L63
Barthelmy, S. D., Barbier, L. M., Cummings, J. R., et al. 2005, SSRv, 120, 143
Becker, A. C., Wittman, D. M., Boeshaar, P. C., et al. 2004, ApJ, 611, 418
Benz, A. O., Fuerst, E., & Kiplinger, A. L. 1983, Natur, 302, 45
Benz, A. O., Gudel, M., & Mattei, J. A. 1996, in ASP Conf. Ser. 93, Radio Emission from the Stars and the Sun, ed. A. R. Taylor & J. M. Paredes (San Francisco, CA: ASP), 188
Berger, E. 2002, ApJ, 572, 503
Berger, E. 2006, ApJ, 648, 629
Berger, E., Ball, S., Becker, K. M., et al. 2001, Natur, 410, 338
Berger, E., Basri, G., Fleming, T. A., et al. 2010, ApJ, 709, 332
Berger, E., Basri, G., Gizis, J. E., et al. 2008a, ApJ, 676, 1307
Berger, E., Fong, W., Sanders, N., & Chornock, R. 2012a, ATel, 4619, 1
Berger, E., Gizis, J. E., Giampapa, M. S., et al. 2008b, ApJ, 673, 1080
Berger, E., Kulkarni, S. R., Frail, D. A., & Soderberg, A. M. 2003, ApJ, 599, 408
Berger, E., Rutledge, R. E., Phan-Bao, N., et al. 2009, ApJ, 695, 310
Berger, E., Rutledge, R. E., Reid, I. N., et al. 2005, ApJ, 627, 960
Berger, E., Zauderer, A., Pooley, G. G., et al. 2012b, ApJ, 748, 36
Bertin, E., Mellier, Y., Radovich, M., et al. 2002, in ASP Conf. Ser. 281, Astronomical Data Analysis Software and Systems XI, ed. D. A. Bohlender, D. Durand, & T. H. Handley (San Francisco, CA: ASP), 228
Blandford, R. D., & McKee, C. F. 1976, PhFl, 19, 1130
Blanton, M. R., & Roweis, S. 2007, AJ, 133, 734
Bloom, J. S., Giannios, D., Metzger, B. D., et al. 2011, Sci, 333, 203
Bloom, J. S., Kulkarni, S. R., & Djorgovski, S. G. 2002, AJ, 123, 1111
Bloom, J. S., Richards, J. W., Nugent, P. E., et al. 2012, PASP, 124, 1175
Bloom, J. S., Starr, D. L., Blake, C. H., Skrutskie, M. F., & Falco, E. E. 2006, in ASP Conf. Ser. 351, Astronomical Data Analysis Software and Systems XV, ed. C. Gabriel, C. Arviset, D. Ponz, & S. Enrique (San Francisco, CA: ASP), 751
Burgasser, A. J., & Putman, M. E. 2005, ApJ, 626, 486
Burrows, D. N., Hill, J. E., Nousek, J. A., et al. 2005, SSRv, 120, 165

Burrows, D. N., Kennea, J. A., Ghisellini, G., et al. 2011, Natur, 476, 421
Butler, N. R., Bloom, J. S., & Poznanski, D. 2010, ApJ, 711, 495
Butler, N. R., & Kocevski, D. 2007, ApJ, 663, 407
Butler, N. R., Kocevski, D., Bloom, J. S., & Curtis, J. L. 2007, ApJ, 671, 656
Cannizzo, J. K. 1993, in The Limit Cycle Instability in Dwarf Nova Accretion Disks, ed. J. C. Wheeler (Singapore: World Scientific), 6
Cardelli, J. A., Clayton, G. C., & Mathis, J. S. 1989, ApJ, 345, 245
Cenko, S. B., Kelemen, J., Harrison, F. A., et al. 2009, ApJ, 693, 1484
Cenko, S. B., Krimm, H. A., Horesh, A., et al. 2012, ApJ, 753, 77
Chakraborti, S., & Ray, A. 2011, ApJ, 729, 57
Chandra, P., & Frail, D. A. 2012, ApJ, 746, 156
Charles, P. A., & Coe, M. J. 2006, Optical, Ultraviolet and Infrared Observations of X-Ray Binaries, ed. W. H. G. Lewin & M. van der Klis (Cambridge: Cambridge Univ. Press), 215
Chevalier, R. A., & Li, Z.-Y. 2000, ApJ, 536, 195
Cobb, B. E., Bailyn, C. D., van Dokkum, P. G., & Natarajan, P. 2006, ApJL, 645, L113
Corbel, S., Nowak, M. A., Fender, R. P., Tzioumis, A. K., & Markoff, S. 2003, A&A, 400, 1007
Cordes, J. M., & Lazio, T. J. W. 2002, arXiv:astro-ph/0207156
Curran, P. A., Evans, P. A., de Pasquale, M., Page, M. J., & van der Horst, A. J. 2010, ApJL, 716, L135
Dahn, C. C., Harris, H. C., Vrba, F. J., et al. 2002, AJ, 124, 1170
Dermer, C. D., Chiang, J., & Mitman, K. E. 2000, ApJ, 537, 785
Drake, A. J., Djorgovski, S. G., Mahabal, A., et al. 2009, ApJ, 696, 870
Dressler, A., Bigelow, B., Hare, T., et al. 2011, PASP, 123, 288
Esin, A. A., McClintock, J. E., & Narayan, R. 1997, ApJ, 489, 865
Falcke, H., Körding, E., & Markoff, S. 2004, A&A, 414, 895
Fender, R. P., Belloni, T. M., & Gallo, E. 2004, MNRAS, 355, 1105
Gallo, E., Fender, R. P., & Pooley, G. G. 2003, MNRAS, 344, 60
Gal-Yam, A., Ofek, E. O., Filippenko, A. V., Chornock, R., & Li, W. 2002, PASP, 114, 587
Gal-Yam, A., Ofek, E. O., Poznanski, D., et al. 2006, ApJ, 639, 331
Gehrels, N., Chincarini, G., Giommi, P., et al. 2004, ApJ, 611, 1005
Geldzahler, B. J., Johnston, K. J., Spencer, J. H., et al. 1983, ApJL, 273, L65
Ghirlanda, G., Nava, L., Ghisellini, G., et al. 2012, MNRAS, 420, 483
Granot, J., Panaitescu, A., Kumar, P., & Woosley, S. E. 2002, ApJL, 570, L61
Granot, J., & Piran, T. 2012, MNRAS, 421, 570
Güdel, M. 2002, ARA&A, 40, 217
Guetta, D., & Della Valle, M. 2007, ApJL, 657, L73
Hallinan, G., Bourke, S., Lane, C., et al. 2007, ApJL, 663, L25
Hogg, D. W., Pahre, M. A., McCarthy, J. K., et al. 1997, MNRAS, 288, 404
Huang, Y. F., Dai, Z. G., & Lu, T. 2002, MNRAS, 332, 735
Hurley, K., Golenetskii, S., Aptekar, R., et al. 2010, in AIP Conf. Proc. 1279, Deciphering the Ancient Universe with Gamma-Ray Bursts, ed. N. Kawai & S. Nagataki (Melville, NY: AIP), 330
Hynes, R. I., Mauche, C. W., Haswell, C. A., et al. 2000, ApJL, 539, L37
Ivezic, Z., Tyson, J. A., Acosta, E., et al. 2008, arXiv:0805.2366
Jakobsson, P., Hjorth, J., Malesani, D., et al. 2012, ApJ, 752, 62
Kaiser, N., Burgett, W., Chambers, K., et al. 2010, Proc. SPIE, 7733, 77330
Kann, D. A., Klose, S., Zhang, B., et al. 2010, ApJ, 720, 1513
King, A. R., & Ritter, H. 1998, MNRAS, 293, L42
Körding, E., Rupen, M., Knigge, C., et al. 2008, Sci, 320, 1318
Kulkarni, S. R., Frail, D. A., Wieringa, M. H., et al. 1998, Natur, 395, 663
Kulkarni, S. R., & Rau, A. 2006, ApJL, 644, L63
Law, N. M., Kulkarni, S. R., Dekany, R. G., et al. 2009, PASP, 121, 1395
Levan, A. J., Tanvir, N. R., Cenko, S. B., et al. 2011, Sci, 333, 199
Levinson, A., Ofek, E. O., Waxman, E., & Gal-Yam, A. 2002, ApJ, 576, 923
Levitan, D., Fulton, B. J., Groot, P. J., et al. 2011, ApJ, 739, 68
Li, W., Chornock, R., Leaman, J., et al. 2011, MNRAS, 412, 1473
Lister, M. L., Cohen, M. H., Homan, D. C., et al. 2009, AJ, 138, 1874
Lithwick, Y., & Sari, R. 2001, ApJ, 555, 540
Lovell, J. E. J., Rickett, B. J., Macquart, J.-P., et al. 2008, ApJ, 689, 108
Lyutikov, M., & Blandford, R. 2003, arXiv:astro-ph/0312347
MacLeod, C. L., Ivezić, Ž., Sesar, B., et al. 2012, ApJ, 753, 106
Madore, B. F., & Arp, H. C. 1979, ApJL, 227, L103
Mahabal, A., Drake, A., Djorgovski, S. G., et al. 2012, ATel, 4586, 1
Malacrino, F., Atteia, J. L., Boër, M., et al. 2007, A&A, 464, 29
McLean, M., Berger, E., & Reiners, A. 2012, ApJ, 746, 23
Meegan, C., Lichti, G., Bhat, P. N., et al. 2009, ApJ, 702, 791
Metzger, B. D., & Berger, E. 2012, ApJ, 746, 48
Metzger, B. D., Giannios, D., & Mimica, P. 2012, MNRAS, 420, 3528
Mirabel, I. F., Dhawan, V., Mignani, R. P., Rodrigues, I., & Guglielmetti, F. 2001, Natur, 413, 139
Mirabel, I. F., & Rodríguez, L. F. 1999, ARA&A, 37, 409
Muno, M. P., Belloni, T., Dhawan, V., et al. 2005, ApJ, 626, 1020
Nakar, E., & Piran, T. 2003, NewA, 8, 141
Nakar, E., & Piran, T. 2011, Natur, 478, 82
Nakar, E., Piran, T., & Granot, J. 2002, ApJ, 579, 699
Nysewander, M., Fruchter, A. S., & Pe'er, A. 2009, ApJ, 701, 824
Oates, S. R., Page, M. J., Schady, P., et al. 2009, MNRAS, 395, 490
Ofek, E. O., Laher, R., Law, N., et al. 2012, PASP, 124, 62
Oke, J. B., Cohen, J. G., Carr, M., et al. 1995, PASP, 107, 375
Oke, J. B., & Gunn, J. E. 1983, ApJ, 266, 713
Panaitescu, A., & Kumar, P. 2001a, ApJL, 560, L49
Panaitescu, A., & Kumar, P. 2001b, ApJ, 554, 667
Panaitescu, A., & Vestrand, W. T. 2008, MNRAS, 387, 497
Patten, B. M., Stauffer, J. R., Burrows, A., et al. 2006, ApJ, 651, 502
Perley, R. A., Chandler, C. J., Butler, B. J., & Wrobel, J. M. 2011, ApJL, 739, L1
Perna, R., & Loeb, A. 1998, ApJL, 509, L85
Piran, T. 2004, RvMP, 76, 1143
Rahmer, G., Smith, R., Velur, V., et al. 2008, Proc. SPIE, 7014, 70144
Ramsay, G., Barclay, T., Steeghs, D., et al. 2012, MNRAS, 419, 2836
Rau, A., Greiner, J., & Schwarz, R. 2006, A&A, 449, 79
Rau, A., Kulkarni, S. R., Law, N. M., et al. 2009, PASP, 121, 1334
Rau, A., Ofek, E. O., Kulkarni, S. R., et al. 2008, ApJ, 682, 1205
Rau, A., Schwarz, R., Kulkarni, S. R., et al. 2007, ApJ, 664, 474
Readhead, A. C. S. 1994, ApJ, 426, 51
Reddy, N. A., Steidel, C. C., Pettini, M., et al. 2008, ApJS, 175, 48
Remillard, R. A., & McClintock, J. E. 2006, ARA&A, 44, 49
Rhoads, J. E. 1997, ApJL, 487, L1
Rhoads, J. E. 1999, ApJ, 525, 737
Rhoads, J. E. 2003, ApJ, 591, 1097
Rickett, B. J. 1990, ARA&A, 28, 561
Route, M., & Wolszczan, A. 2012, ApJL, 747, L22
Rykoff, E. S., Aharonian, F., Akerlof, C. W., et al. 2005, ApJ, 631, 1032
Rykoff, E. S., Aharonian, F., Akerlof, C. W., et al. 2009, ApJ, 702, 489
Sari, R., Piran, T., & Halpern, J. P. 1999, ApJL, 519, L17
Sari, R., Piran, T., & Narayan, R. 1998, ApJL, 497, L17
Sault, R. J., Teuben, P. J., & Wright, M. C. H. 1995, in ASP Conf. Ser. 77, Astronomical Data Analysis Software and Systems IV, ed. R. A. Shaw, H. E. Payne, & J. J. E. Hayes (San Francisco, CA: ASP), 433
Schlegel, D. J., Finkbeiner, D. P., & Davis, M. 1998, ApJ, 500, 525
Shen, R., Kumar, P., & Robinson, E. L. 2006, MNRAS, 371, 1441
Skrutskie, M. F., Cutri, R. M., Stiening, R., et al. 2006, AJ, 131, 1163
Soderberg, A. M., Chakraborti, S., Pignata, G., et al. 2010, Natur, 463, 513
Soderberg, A. M., Kulkarni, S. R., Nakar, E., et al. 2006a, Natur, 442, 1014
Soderberg, A. M., Nakar, E., Berger, E., & Kulkarni, S. R. 2006b, ApJ, 638, 930
Spergel, D. N., Bean, R., Doré, O., et al. 2007, ApJS, 170, 377
Starling, R. L. C., van der Horst, A. J., Rol, E., et al. 2008, ApJ, 672, 433
Tanaka, Y., & Shibazaki, N. 1996, ARA&A, 34, 607
Tody, D. 1986, Proc. SPIE, 627, 733
Tomsick, J. A., Halpern, J. P., Kemp, J., & Kaaret, P. 1999, ApJ, 521, 341
Uemura, M., Kato, T., Matsumoto, K., et al. 2000, PASJ, 52, L15
Vanden Berk, D. E., Lee, B. C., Wilhite, B. C., et al. 2002, ApJ, 576, 673
van Eerten, H., van der Horst, A., & MacFadyen, A. 2012, ApJ, 749, 44
van Eerten, H., Zhang, W., & MacFadyen, A. 2010, ApJ, 722, 235
van Paradijs, J., & White, N. 1995, ApJL, 447, L33
van Velzen, S., Körding, E., & Falcke, H. 2011, MNRAS, 417, L51
Voges, W., Aschenbach, B., Boller, T., et al. 1999, A&A, 349, 389
Wagner, R. M., Foltz, C. B., Shahbaz, T., et al. 2001, ApJ, 556, 42
Walker, M. A. 1998, MNRAS, 294, 307
White, N. E., & van Paradijs, J. 1996, ApJL, 473, L25
Wilson, J. C., Eikenberry, S. S., Henderson, C. P., et al. 2003, Proc. SPIE, 4841, 451
Woosley, S. E., & Bloom, J. S. 2006, ARA&A, 44, 507
Wygoda, N., Waxman, E., & Frail, D. A. 2011, ApJL, 738, L23
Yost, S. A., Harrison, F. A., Sari, R., & Frail, D. A. 2003, ApJ, 597, 459
Zauderer, B. A., Berger, E., Soderberg, A. M., et al. 2011, Natur, 476, 425
Zhang, W., & MacFadyen, A. 2009, ApJ, 698, 1261
Zurita, C., Casares, J., Shahbaz, T., et al. 2000, MNRAS, 316, 137